EINDHOVEN UNIVERSITY OF TECHNOLOGY

Eindhoven University of Technology

MASTER

Injection of hydrogen-free carbon in Ar-N2 plasmas for the deposition of carbon nitride

van Deurzen, P.D.J.

Award date:
1997

Link to publication

Disclaimer
This document contains a student thesis (bachelor's or master's), as authored by a student at Eindhoven University of Technology. Student theses are made available in the TU/e repository upon obtaining the required degree. The grade received is not published on the document as presented in the repository. The required complexity or quality of research of student theses may vary by program, and the required minimum study period may vary in duration.

General rights
Copyright and moral rights for the publications made accessible in the public portal are retained by the authors and/or other copyright owners and it is a condition of accessing publications that users recognise and abide by the legal requirements associated with these rights.

- Users may download and print one copy of any publication from the public portal for the purpose of private study or research.
- You may not further distribute the material or use it for any profit-making activity or commercial gain

Injection of hydrogen-free carbon in Ar-N_2 plasmas for the deposition of carbon nitride

P.D.J. van Deurzen

October 1997
VDF/NT 97-41

Report of a graduation project.
Supervisors:
drs. A. de Graaf
dr. ir. M.C.M. van de Sanden
prof. dr. ir. D.C. Schram

Summary

Carbon nitride films have properties which make them highly interesting for the industry. The aim of this research is the deposition of carbon nitride films with an expanding arc plasma. To prevent incorporation of hydrogen, two methods to inject hydrogen-free carbon in plasmas have been developed: injection of fullerene or graphite vapor in the plasma beam, and using a graphite containing nozzle in the arc instead of the copper nozzle.

To study the influence of these methods on plasmas, first argon-nitrogen plasmas have been studied. In these plasmas, a decrease of the electron density with increasing nitrogen concentration is observed. This decrease is caused by charge transfer reactions, leading to the formation of molecular nitrogen ions, which fastly recombine with electrons, leading to the loss of ions and electrons. Furthermore, in argon-nitrogen plasmas are the electron temperature and the vibrational temperature ($\approx$0.50 eV) higher than in pure argon plasmas ($\approx$0.27 eV). This may be caused by transfer of energy from metastable nitrogen species to the electrons by super elastic collisions, or by the recombination of N_2^+ ions mainly taking place with low energy electrons, leaving the electrons with higher energy inside the plasma. These electrons with higher energy can more easily excite the vibrational levels of nitrogen molecules, leading to a higher vibrational temperature.

When fullerene vapor is injected in an argon plasma, C_2 molecules are observed, caused by the fragmentation of fullerene. The amount of C_2 inside the plasma is proportional to the vapor pressure of fullerene inside the evaporator. Because the fullerene lies on the wall of a cylinder, the evaporation surface changes in time, and as a result, also the amount of fullerene injected in the plasmas. When graphite powder is heated to 1000^{0}C, also carbon species are observed, in spite of the low vapor pressure at this temperature. This might be explained by the breaking of weak bondings between clusters of carbon.

When a graphite containing nozzle is used to create argon-nitrogen plasmas, nitrogen chemically etches the nozzle, forming CN molecules. If we compare the vibrational temperature of the molecules with the vibrational temperature inside argon-nitrogen plasmas created with a copper nozzle, the same values are observed, only shifted to a higher nitrogen concentration in the former case. This shift is caused by the loss of nitrogen in the formation of CN. In the films deposited with argon-nitrogen plasmas created with a graphite containing nozzle, different CN bondings are observed. The refractive index of the films changes from 1.93 when a new nozzle is used, to 1.79 when an old nozzle is used. The deposition rate is with approximately 0.3 nm/s, lower than for deposition of amorphous hydrogenated carbon nitride films with the cascaded arc.

Contents

1 Introduction **1**

2 The deposition setup **5**

3 Diagnostics **7**
3.1 Langmuir probes 7
3.2 Optical Emission Spectroscopy 11
3.3 Fourier transform infrared spectroscopy 14
3.4 Ellipsometry 16

4 Argon-nitrogen plasmas **19**
4.1 Model for argon-nitrogen plasmas 20
4.2 Electron densities 22
4.3 Electron temperatures 27
4.4 Emission spectroscopy 32
4.5 Rotational and vibrational temperatures 33

5 The evaporator **35**
5.1 Setup of the evaporator 35
5.2 Evaporation rate of C_{60} 37
5.3 Fullerene 38
5.4 Graphite 42

6 Graphite containing nozzle **45**
6.1 Setup of the graphite containing nozzle 45
6.2 Emission spectroscopy 46
6.3 Rotational and vibrational temperatures 51
6.4 Film characterization 53

7 Conclusions **61**

Technology assessment 65

Bibliography 66

Appendices

A The flow controller for the evaporator 71
A.1 Operating the flow controller 71
A.2 Calibration of the flow controller 72

B Operating box for the evaporator 75

C Listing for the Ar-N_2 model 77

Chapter 1

Introduction

The industry is highly interested in films with properties like extreme hardness, wear resistance, chemical inertness, optical tunability, infra red transparency and high thermal conductivity. Some of these materials, such as diamond like carbon, amorphous carbon, boron carbide and boron nitride, are already being synthesized with a large economical impact. The study of carbon nitride started only very recently. The interest in this material was initiated by publications of Liu and Cohen [1], predicting from ab initio electron structure calculations, that carbon nitride may be harder than diamond. Carbon nitride is the only compound that is expected to have low deposition temperature (300^0C - 500^0C), ultra-high hardness, large band-gap (6 eV), high thermal conductivity (15 W cm^{-1} K^{-1}) and good surface roughness linked. As a consequence it has great potential for applications like tribological coatings, high density storage, hard disk manufacturing, cutting tools, thermal management of microelectronics components, and (infra red) optics.

Carbon nitride may exist in different forms like α-C_3N_4, β-C_3N_4, cubic-C_3N_4, pseudo-cubic-C_3N_4, rhombohedrical-C_3N_4 and graphite-C_3N_4. These types consist of C-N networks with varying ratios of sp^2 and sp^3 bondings, resulting in different properties. Three types of C_3N_4 are given in figure 1.1.

Since the publication of Liu and Cohen many attempts have been made to synthesize carbon nitride. Most of these studies are in a non co-operative way. Under supervision of the Foundation for Fundamental Research of Matter (FOM), a framework of contacts between research teams and possibly interested industries has been initiated. The group Equilibrium and Transport in Plasmas (ETP) at the Eindhoven University of Technology operates within this framework. This group also operates within the European Carbon Nitride Network, in which 5 research institutes are assembled. The aim of the research at the group ETP, is deposition of carbon nitride films with an expanding arc plasma and the characterization of the deposition plasmas and the films. The deposition of amorphous hydrogenated carbon nitride films has already been studied. The results of these studies are presented in [2].

Most of the methods used for deposition of films (e.g. Plasma Vapor Deposition [3], Plasma Enhanced Chemical Vapor Deposition [4]) yield a limited amount of incorporation of nitrogen (20% to 40%), a low growth rate (3 nm/min) and in most cases films which

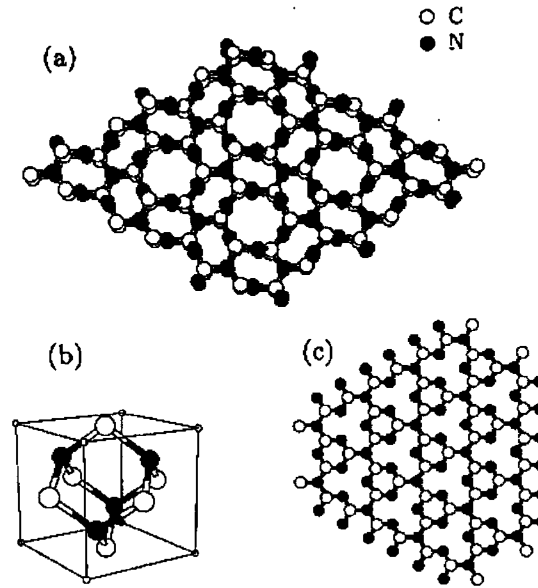

Figure 1.1: Three different forms of C_3N_4: a) β-C_3N_4; b) cubic-C_3N_4; and c) graphite-C_3N_4

are amorphous. In a few cases evidence for the formation of crystalline carbon nitride is found [47] [48]. With an expanding arc plasma it is possible to provide plasmas with large concentrations of atomic nitrogen. The plasma is created in a cascaded arc at high pressure ($\approx$ 0.4 bar) and expands in a vessel at low pressure. Here gas or vapor can be admixed, which reacts with the plasma. The plasma with the created reaction products flows to a substrate where the deposition takes place. This technique has been used successfully to deposit covalent materials such as a-C:H, a-Si:H, and graphite with growth rates 10 to 20 times higher as with other methods [5]. Another advantage of this technique is the spatial separation of plasma creation, plasma transport and deposition. This enables a separate optimalization of these three processes.

Earlier study [2] show that if during the deposition hydrogen is present in the plasma, it can incorporate in the growing carbon nitride film. The hydrogen causes the termination of dangling bonds in the layer, preventing a long-range three dimensional bonded structure [6]. This results in a lower hardness of the films.

To minimize the effect of hydrogen on the formation of carbon nitride, two methods to get hydrogen-free carbon inside the plasmas are studied in the group Equilibrium and Transport in Plasmas. The first method consists of connecting an evaporator to the expansion vessel to inject fullerene (C_{60}) or graphite vapor into expanding argon-nitrogen plasmas. This method is described in §5.1. The second method, which is described in §6.1, consists of replacing the copper nozzle, normally used in the cascaded arc, with a graphite containing nozzle.

To study the influence of these methods on different argon-nitrogen plasmas, first the argon-nitrogen plasmas have been examined. These plasmas are investigated with Lang-

muir probe measurements (§3.1) and optical emission spectroscopy (§3.2) and the results are compared with a theoretical model (§4.1). The results and a possible explanation of the behaviour of these argon-nitrogen plasmas will be given in chapter 4.

In chapter 5 the effect of fullerene and graphite, injected with the evaporator, on pure argon plasmas will be examined. Also the differences between the use of fullerene and of graphite will be discussed.

Furthermore, different plasmas created with a graphite containing nozzle are studied with optical emission spectroscopy. In §6.2 the results will be discussed and compared with plasmas created with the nozzle normally used. The graphite containing nozzle is also used for deposition of carbon nitride layers. The growth rates and the refractive indices of these layers are deduced with ellipsometry (§3.4) and the different bondings in the layers are examined with Fourier transform infrared absorption spectroscopy (§3.3). In §6.4 these results will be discussed.

In chapter 2 the deposition setup present in the DEPO I laboratory is described. The theoretical model used to compare the results of the argon-nitrogen plasmas with, is described in §4.1. The used diagnostic techniques (Langmuir probe, optical emission spectroscopy, Fourier transform infrared absorption spectroscopy and ellipsometry) are explained in chapter 3.

Chapter 2

The deposition setup

A schematic drawing of the plasma beam deposition setup is shown in figure 2.1. The setup consists of a cascaded arc, an expansion vessel, a substrate holder and a pumping system. The experiment is controlled via a Programmable Logical Control (PLC) unit which is operated via Intouch software on a personal computer.

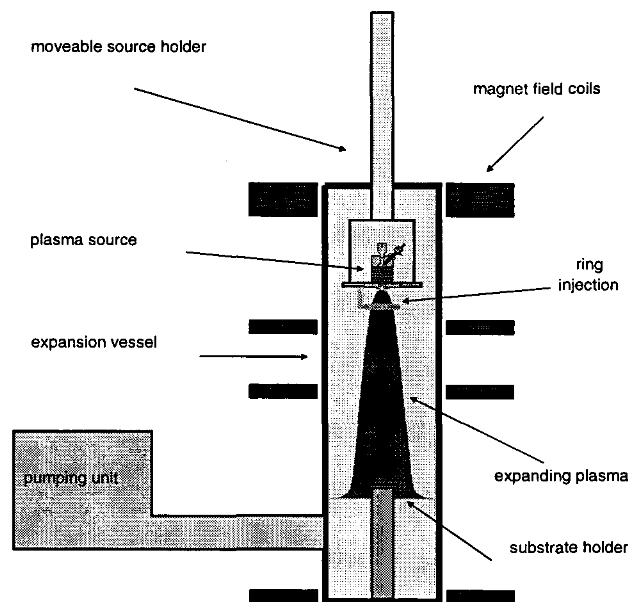

Figure 2.1: Deposition setup

The plasma is created in the cascaded arc, which is placed in a moveable source holder. The cascaded arc consists of three cathodes, an anode and four water-cooled circular copper plates, separated by an insulator. The plates all have a central bore of 4 mm which forms the plasma channel. An argon-nitrogen mixture is injected at the cathode side, flows to the anode and is ionized by a dc discharge. The ionization degree depends on the arc power, the composition of the mixture and the total flow. In standard conditions the flow

is 100 scc/s[1]. The plasma expands supersonically in the vessel, which is at much lower pressure (± 0.25 mbar) than the arc (± 400 mbar). This results in a stationary shock at ± 5 cm downstream. After this shock the plasma flows with subsonic velocities (500 - 1000 m/s) towards the substrate holder. On this holder substrates (usually crystalline silicon) of 2.5 cm × 2.5 cm can be mounted. The temperature of the substrate holder can be regulated, and due to a helium flow, which insures a good thermal contact, a maximum temperature difference between the substrate and the holder of 10^0C is achieved [7]. With the movable source holder the distance between the plasma source and the substrate can be varied between 65 and 5 cm. The pressure in the expansion vessel is controlled with a vacuum pumping system, consisting of two mechanical booster pumps (Edwards EH2600: 2600 m^3/hr; Edwards EH500A: 500 m^3/hr) and a rotary piston pump (Edwards: 240 m^3/hr).

With this deposition setup several plasmas have been examined: argon-nitrogen plasmas of different compositions, argon plasmas with fullerene vapor (C_{60}), argon plasmas with graphite vapor, and argon-nitrogen plasmas which have been created in a cascaded arc with a graphite containing nozzle (see §6.1). The settings used during these experiments are given in table 2.1.

Table 2.1: Settings used during the experiments.

	Ar+N_2	Ar+C_{60}	Ar+graphite	Nozzle
Total flow[2] (scc/s)	100	35	35	100
N_2 flow (scc/s)	0-20	-	-	0-20
Ar flow through the evaporator (scc/s)	-	10	10	-
I_{arc} (A)	48;75;87	30	35	48;75;87
p_{arc} (bar)	0.5	0.1	0.1	0.5
p_{vessel} (mbar)	0.25	0.15	0.15	0.25
distance to subst(cm)	65-40	42	42	65
$T_{substrate}$(^{0}C)	50	-	-	50

[1] 1 scc/s = 1 cm^3 per second at atmospheric pressure and room temperature
[2] without fullerene or graphite vapor

Chapter 3

Diagnostics

In this chapter the used diagnostic methods will be described. The argon-nitrogen plasmas are analyzed with a Langmuir probe (§3.1) to determine the electron temperature and density. With optical emission spectroscopy (§3.2) the excited particles present in the different plasmas and the rovibrational temperatures are determined. The deposited films are analyzed with infrared spectroscopy (§3.3) to investigate the different atomic bondings, and during growth with ellipsometry (§3.4) to determine the growth rate and the refractive index.

3.1 Langmuir probes

A Langmuir probe is a small electrical conductor, which is immersed in a plasma. These probes are used in evaluating important plasma parameters, such as the electron and ion density and electron temperature. The measurements are based on the principle that the current collected by a conductor inside a plasma, depends on:

- electron density (n_e)
- ion density (n_i)
- velocity distribution of the electrons
- potential applied to the probe (V_{probe})

An advantage of probes is the ability to make localized measurements because of the small size of the probe. A disadvantage is that the probe is situated in the plasma and thus forms a boundary to the plasma. This boundary may affect the surrounding volume. At this boundary a layer called "sheath" is formed, in which electron and ion densities are different from the plasma.

Irving Langmuir was one of the first who used probes as a means of plasma diagnostics. He developed a relatively simple self-consistent theory, which forms the basis of all

considerations with regard to probes [12]. In the theory used, a couple of assumptions are made [13]:

- quasi-neutrality inside the plasma ($n_i = n_e$),
- mean free paths of the electrons and ions are larger than the radius of the probe,
- probe radius $\gg$ the radius of the smallest sphere in which the plasma can be considered quasi-neutral, the Debye length, $\lambda_D = \sqrt{(\epsilon_0 k T_e)/(n_e e^2)}$
- velocity distribution of the ions and electrons is Maxwellian,

During the experiments, the probe radius is 0.20 mm, the mean free path of the particles ($n_e < 10^{20}$ m^{-3}, $\sigma < 10^{-18}$ m^2) is larger than 10 mm and the Debye length ($T_e < 1$ eV, $n_e > 10^{18}$ m^{-3}) is smaller than 7×10^{-3} mm. The slope of the logarithm of the electron current (I_e) plotted against the probe potential, is constant in our experiments. Hence, as will be stated later in this section, the velocity distribution of the electrons is Maxwellian. The assumptions are thus satisfied.

For a Maxwellian velocity distribution the mean speed of a particle (v_{mean}) is given by:

$$v_{mean} = \sqrt{\frac{8kT}{\pi m}} \tag{3.1}$$

with k the Boltzmann constant, T_e the electron temperature and m the mass of the particle.

The probe is also assumed to be a perfect absorber. All the charge entering the sheath will impinge on the probe. Therefore, there must be a current flowing to the probe to prevent accumulation of charge. This current I is proportional to the particle flux ϕ:

$$I = -q\phi \tag{3.2}$$

with q the charge of the particle.

If these conditions are met, by plotting the measured current against the probe potential (a so called IV-characteristic), the other parameters (n_e, T_e) can be defined. Figure 3.1 is an example of such an IV-characteristic. Negative current is plotted against the probe voltage.

When the probe is floating (i.e. disconnected from an external voltage supply) the probe current is zero. Hence, the numbers of electrons and ions arriving at the probe per unit of time, have to be equal. Because of the much smaller mass of the electrons compared to that of the ions, the mean velocity of the electrons will exceed that of the ions (see Eq. 3.1). The densities of the electrons and ions are equal outside the sheath. Hence, initially more electrons than ions hit the probe per unit of time, and negative charge accumulates on the probe, repelling the electrons and accelerating the ions. This negative charge grows until no resultant current flows to the probe, and the floating potential V_{float} is reached.

When the probe potential is negative in respect to the floating potential, less electrons and more ions will reach the probe. If the probe potential is sufficiently negative, no

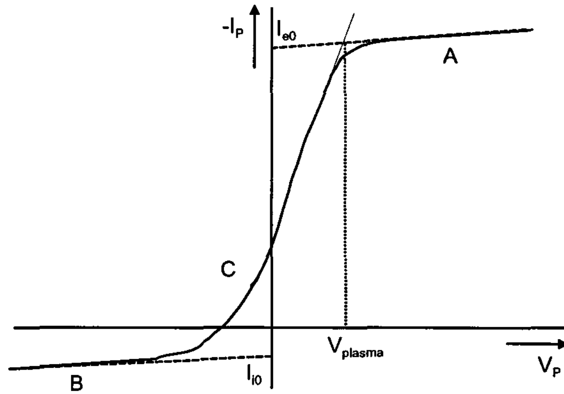

Figure 3.1: Characteristic of a single probe measurement

electrons will reach the probe, while all ions passing the sheath are absorbed. The probe current is then equal to the ion saturation current I_{i0}.

V_{plasma} is the local potential inside the plasma. At this point the potential of the probe is equal to the plasma potential, so no sheath is present. The probe current is the sum of all electrons and ions impinging on the probe by virtue of their thermal motion:

$$I_{probe} = I_{e0} + I_{i0} \tag{3.3}$$

If the probe potential is positive in respect to the plasma potential, the positive ions will be repelled from and the electrons will be accelerated towards the probe. If the energy of the ions is too small to overcome the difference in potential, only the electron current will remain. This is called the electron saturation current I_{e0}. Any further growth of the potential will lead to a slight increase of the electron current due to the enlargement of the sheath.

When the probe potential is decreased in respect to the plasma potential, the transition region will be entered. Here, all ions entering the sheath will impinge on the probe, and less and less electrons are able to overcome the retarding potential ($I_{probe} = I_{i0} + I_e$). Because of their Maxwellian velocity distribution, the density of the electrons at the probe will be governed by Boltzmann's law, so the electron current in this transition region is given by [13]:

$$I_e = I_{e0} \exp(\frac{e(V_{probe} - V_{plasma})}{kT_e}) \tag{3.4}$$

Subtraction of the ion saturation current from the total probe current in the transition region gives the electron current as a function of the probe potential. When the electrons have a Maxwellian distribution, the slope of the logarithm of the electron current (I_e) plotted against the probe potential, is constant. By plotting the logarithm, the electron temperature T_e can be derived:

$$\alpha = \frac{\partial ln I_e}{\partial V_{probe}} = \frac{e}{kT_e} \tag{3.5}$$

In the plasmas used, the velocity distribution is assumed to be Maxwellian and thus isotropic, so the flux of one species of particles to the surface of the probe (A_{probe}) is:

$$\phi = \frac{1}{4} n v_{mean} A_{probe} \tag{3.6}$$

Combining this with 3.1 and 3.2 gives the electron and ion density:

$$n_{e,i} = \frac{4 I_{e,i} \sqrt{\pi m_{e,i}}}{e A_{probe} \sqrt{8kT_e}} \tag{3.7}$$

During the experiments we used a cylindrical probe consisting of a thin tungsten wire (radius 0.20 mm) surrounded by a ceramic insulator. The setup is shown in figure 3.2. The characteristics are obtained by measuring the voltage drop over a resistor as a function of the probe potential with a computer. The characteristics are also recorded with an oscilloscope.

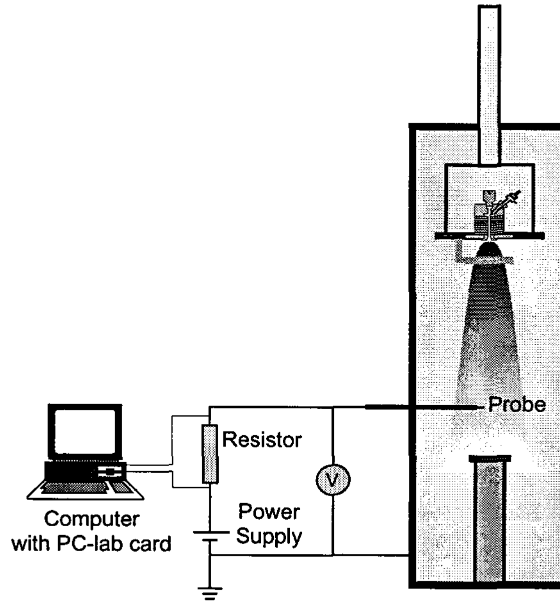

Figure 3.2: Setup of the single probe

To determine the ion density, the mass of the ions which impinge on the probe has to be known (see Eq. 3.7). In the case of pure argon plasmas, the only ions present are Ar^+, so the mass of this ion is used. In the case of Ar/N_2 mixtures also N^+ and N_2^+ impinge on the probe, and for calculation of the ion density, the average mass of all ions impinging on the probe should be used. The amount of the different ions impinging on the probe is, however, unknown so an approximation is used. The ion mass used during the experiments is $m_i = (1-x)m_{Ar} + x m_N$, with x the concentration of the nitrogen flow. When we assume that only Ar^+ and N^+ impinge on the probe and that their relative densities are the same

as inside the arc and thus may be calculated with Eq. 4.1, the ion mass which should be used at a nitrogen concentration of 20%, is 12% lower than the mass we used. However, the ions coming out of the arc will react with the background and their relative densities will change. If we use the program and the reaction rates described in §4.1 to calculate the relative densities at 20 cm from the nozzle, and from these densities the relative ion mass, the ion mass which should be used is 4% lower than we used, at a nitrogen concentration of 20%, leading to an error in the ion density of 2%. Hence, the relative ion mass as calculated in these three methods give a maximum error of 6%, when compared to each other. This is lower than the measuring error, which is 10%-15%. The relative ion mass as calculated in these three methods are given in figure 3.3.

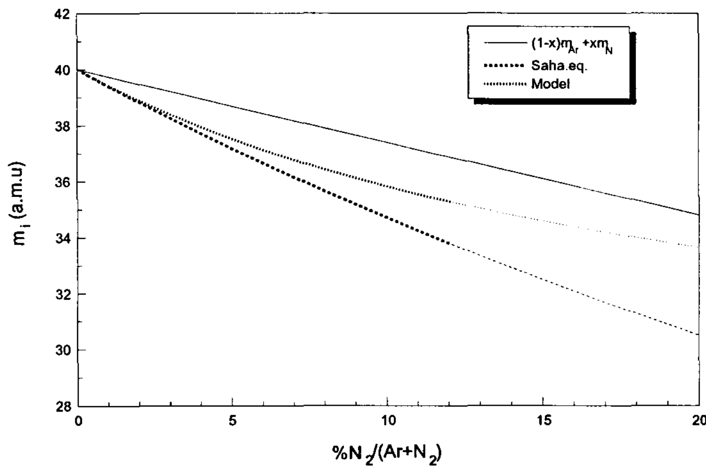

Figure 3.3: Relative ion mass calculated as described above.

3.2 Optical Emission Spectroscopy

In a plasma a part of the atomic and molecular particles will be in an excited state. These particles may decay to a lower state by emission of electromagnetic radiation and the emitted light can be detected. This technique is called optical emission spectroscopy (OES). An advantage of OES is that it is a non-disturbing method. A disadvantage is that only the excited atoms and molecules are detected.

For the atomic species the decay occurs between electronic states. For molecules the total energy is the sum of the electronic, the vibrational and the rotational energies. In correspondence with these three types of energy we can find three types of transitions between energy levels. Transitions between two rotational levels in the same vibrational and electronical level correspond to energy differences in the order of 10^{-3} eV (which corresponds to photons in the far infrared range). An energy difference of about 0.3 eV (in the infrared range) corresponds to transitions between both rotational and vibrational states. In the case of energy differences of several eV (in the visible or ultraviolet range) the electronical transitions are also involved. The electronical and vibrational states of N_2

and CN are given in the potential curves in figure 3.4. The rotational levels are not given in this figure. The dark horizontal lines give the electronic states. The thinner lines give the vibrational levels in each of the electronic states.

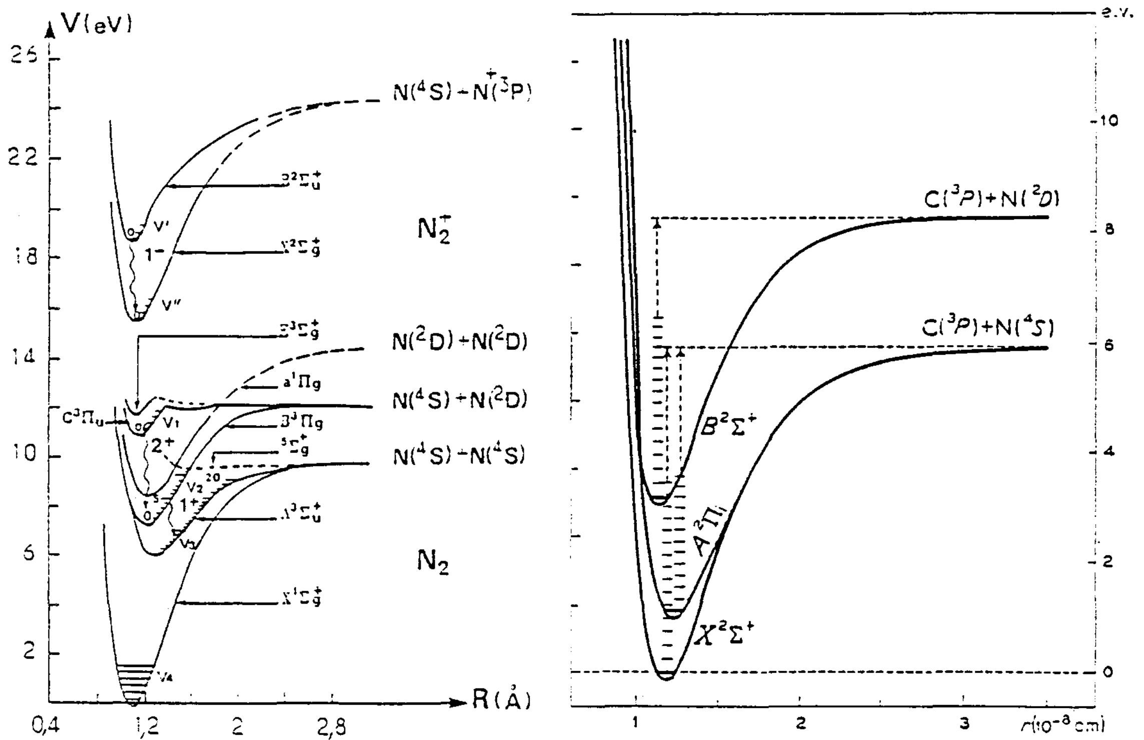

Figure 3.4: Potential curves of N_2 [21] and CN [14].

The emission spectrum of an atom consists of several lines at different wavelength which are characteristic for the transitions in that particular atom. For molecules, like N_2 and CN, the spectrum does not consist of sharp, single lines, but of more or less broad wavelength regions (bands). Each band consists of different rotational and vibrational transitions within one electronic transition. The distribution over the different rotational and vibrational levels depends on the rotational and the vibrational temperatures of the molecules. Apart from the determination of the species present in the plasma and their corresponding excitation energies, the molecular bands can be used to determine the rotational and vibrational temperature of the molecules. For spectra with completely isolated lines the temperatures can be obtained by comparing the intensities I of lines [14]:

$$\sum_{v'} \frac{I(v,v')}{\nu^4} = C_1 \exp[-\frac{Ghc}{kT_{vib}}] \tag{3.8}$$

$$\frac{I}{J+J'+1} = C_2 \exp[-\frac{Fhc}{kT_{rot}}] \tag{3.9}$$

where C_1 and C_2 are constants, depending on the number of particles in the initial state, v and v' the vibrational quantum numbers, G the vibrational term of v (in cm^{-1}), J and J'

the rotational quantum numbers and F the rotational term of J (in cm^{-1}). The vibrational term G is given by:

$$G = \omega(v + \frac{1}{2}) \tag{3.10}$$

where ω is the vibrational frequency in cm^{-1}. The rotational term F is given by:

$$F = \frac{h}{8\pi^2 c I} J(J+1) \tag{3.11}$$

where h is Planck's constant, c the speed of light and I the momentum of inertia of the molecule.

Because molecular emission spectra are composed of several hundreds of lines which overlap, the determination of the rotational and vibrational temperatures is not straightforward. To obtain rotational and vibrational temperatures in this case, simulated and measured molecular spectra have to be compared. The simulation has to follow different steps: calculation of the position of each line, calculation of the intensity of each line at given rotational and vibrational temperatures and a convolution between the ideal spectra and the apparatus profile [15]. After subtraction of the background and continuous plasma emission from the experimental spectrum, the simulated and the experimental spectra can be compared. Aldea *et al.* have developed a computer simulation procedure with which it is possible to obtain the rotational and vibrational temperatures, even in the case the apparatus profile width or the background and continuous plasma emission of the spectra are unknown [16]. This program is used to determine the temperatures for plasmas containing N_2^+ or CN.

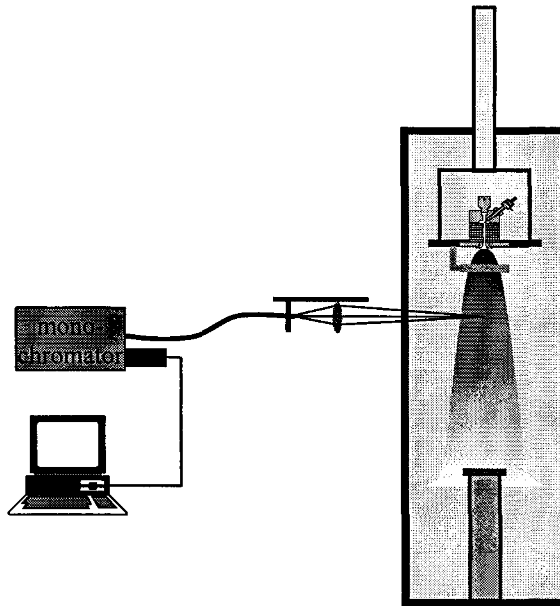

Figure 3.5: Setup of optical emission spectroscopy

A schematic drawing of the optical emission spectroscopy setup is given in figure 3.5. The light from the central axis of the plasma in the vacuum vessel is focussed on the entrance slit of an optical fiber with a lens. The lens can be moved in both vertical and horizontal direction. The light is transported through the fiber to a monochromator. The slit width of the monochromator can be varied. For high spectral resolution the slit has to be small, but to get higher intensity the slit has to be large. During the experiments slits of 50μm and 250μm are used. The wavelength resolved emission intensity is detected by a photomultiplier which is mounted at the exit slit of the monochromator. A discriminator is used to separate the original photon pulses from noise. The resulting NIM pulses are converted into TTL pulses which are counted with a counter-timer card in a personal computer.

3.3 Fourier transform infrared spectroscopy

Infrared transmission-absorption spectroscopy is an ex situ analysis technique which can be used to determine the refractive index, the thickness and the different bonding types of deposited films. A generally applied technique is Fourier transform infrared spectroscopy (FTIR). This technique makes use of broadband parallel infrared light which is irradiated on an interferometer. The incident light beam is separated by a beamsplitter into two beams which pass a different optical path length and are joined again before leaving the interferometer (see figure 3.6). Due to the difference in optical path length, the two beams

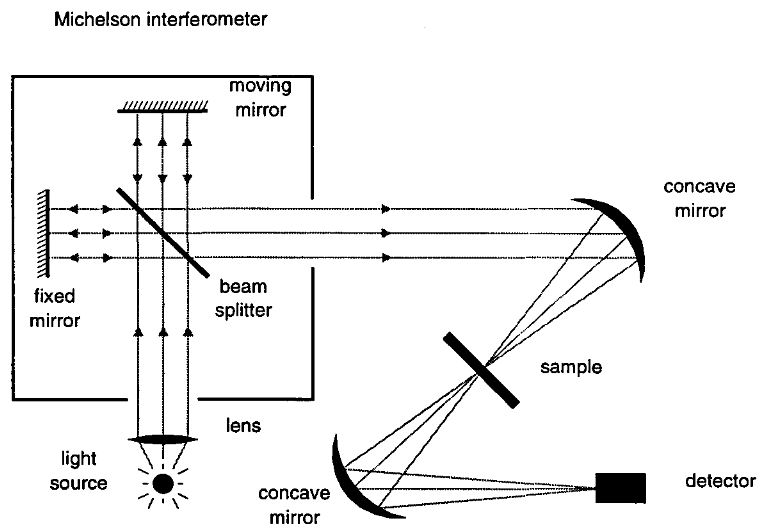

Figure 3.6: Schematic drawing of FTIR spectroscopy setup.

will have a phase difference and as a result they will interfere when they recombine. The phase difference δ depends on the wavenumber ν of the light and is given by:

$$\delta = 2\pi\nu x \tag{3.12}$$

with x the optical path length difference. The beam leaving the interferometer passes the sample, and the transmitted signal is focussed on a detector. The intensity is measured under variation of the optical path length in the interferometer. For a broadband light source the transmitted intensity will consist of a constant and a varying part. The varying part of the intensity is given by:

$$I(x) = \int_0^\infty S(\nu) \cdot \cos\delta \cdot d\nu = \int_0^\infty S(\nu) \cdot \cos(2\pi\nu x) \cdot d\nu \tag{3.13}$$

with $S(\nu)$ the intensity as function of the wavenumber. A spectrum with the transmitted intensity as a function of wavenumber is obtained by Fourier transformation of the resulting intensity - optical path length data:

$$S(\nu) = \int_0^\infty I(x) \cdot \cos(2\pi\nu x) \cdot dx \tag{3.14}$$

The transmission spectrum of a deposited film is obtained by dividing the transmission spectrum of the substrate with the film by the transmission of the bare substrate. Because of the multiple reflections in the film an interference pattern may occur. From this pattern the values of the refractive index n and the thickness d of the film can be obtained. Atomic bondings in the layers having vibration energies in the infrared region cause absorption peaks. When the vibration frequencies for the different bondings are known, the bondings present in the layer can be identified. A typical pattern is shown in figure 3.7.

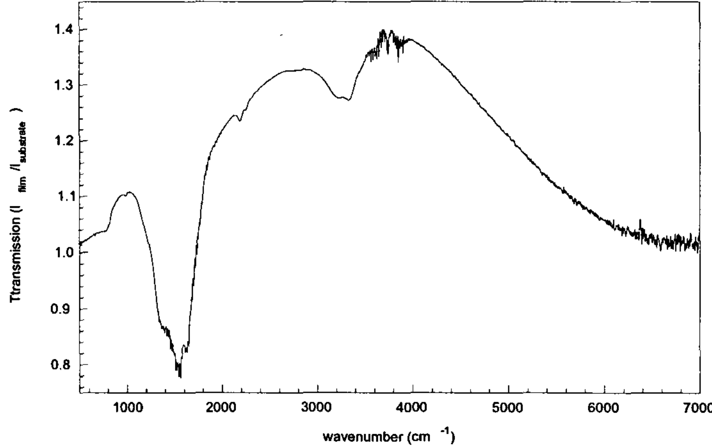

Figure 3.7: Example of a FTIR measurement of an a-C:N film.

By removing the absorption peaks and fitting the curve with the transmission equation derived in [17], the refractive index n and the thickness of the layer d may be obtained:

$$T = \frac{4n^2(n_c + n_0)^2}{(n + n_0)^2(n + n_c)^2}[1 - \frac{2(n - n_c)(n - n_0)}{(n + n_c)(n + n_0)}\cos(4\pi n d\nu) + r_1^2 r_2^2]^{-1} \tag{3.15}$$

with n_0 the refractive index of air (=1), n_c the refractive index of the substrate and r_1 and r_2 the reflection coefficients given in [17].

3.4 Ellipsometry

Ellipsometry is an in situ diagnostic technique used to determine the refractive index and the thickness of a layer during deposition. It is an optical technique which is based on the principle that the reflection coefficient of light polarized parallel to the plane of incidence (p-direction) differs from the reflection coefficient of light polarized perpendicular to the plane of incidence (s-direction). As a consequence the polarization of light changes if it is reflected on a surface. The complex ratio (ρ) between the p- and s-reflection coefficients (r_p and r_s) is used to express this change of polarization:

$$\rho = \frac{r_p}{r_s} = \tan \Psi e^{i\Delta} \tag{3.16}$$

where Ψ and Δ are the two ellipsometric angles which characterize the polarization effects of the surface.

When a thin layer is placed on a substrate the situation becomes more complex, because multiple reflections occur. The netto reflection consists of the direct reflection at the surface of the layer and the contribution of all multiple reflections at the boundary between the layer and the substrate (figure 3.8). The total reflection can be represented by [18]:

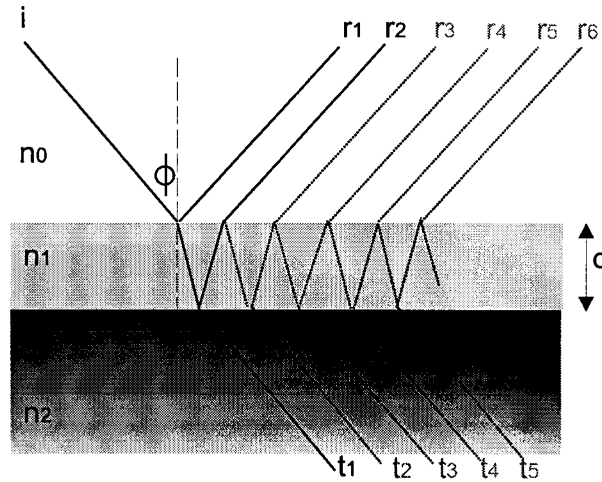

Figure 3.8: Multiple reflections in a thin layer.

$$R = \frac{r_{01} + r_{12}\exp(-2i\beta)}{1 + r_{01}r_{12}\exp(-2i\beta)} \tag{3.17}$$

with β the phase thickness, given by:

$$\beta = \frac{2\pi d}{\lambda}\sqrt{n_1^2 - n_0^2 \sin^2 \phi} \tag{3.18}$$

where d, n_1, ϕ and λ are the thickness of the layer, the refractive index of the layer, the angle of incidence and the wavelength of the light, respectively. These equations are valid for both the p- and s-components and equation 3.16 changes to:

$$\frac{R_p}{R_s} = \tan \Psi e^{i\Delta} \tag{3.19}$$

During a deposition the values for Ψ and Δ change and describe a curve in the $\Psi - \Delta$ plane. The initial values of Ψ and Δ are the values corresponding to the substrate, from which n_2 can be derived. After one revolution of $\Psi\Delta$, β has changed with π. The change in thickness of the depositing layer then can be described by:

$$\Delta d = \frac{\lambda}{2\sqrt{n_1^2 - n_0^2 \sin^2 \phi}} \tag{3.20}$$

From simulations of the total experimental curve, the refractive index n_1 and the thickness d of the layer can be obtained.

A schematic drawing of the setup is given in figure 3.9. Linearly polarized light from a He-Ne laser (Melles Griot 05-LPH-111, λ =632.8 nm) passes a quarter λ plate, resulting in circular polarized light. Next a polarizer changes the light to linear polarized. Then the light passes a rotating compensator before entering the vessel. As a consequence the intensity of the light before reflection, passes through minima and maxima. After reflection the light leaves the vessel, passes an analyzer and reaches a detector. The detector consists of a photodiode, causing a voltage proportional to the intensity of the light. This voltage is stored in a computer, after conversion with an ADC. After calibration the values for Ψ and Δ can be calculated from this data by Fourier analysis.

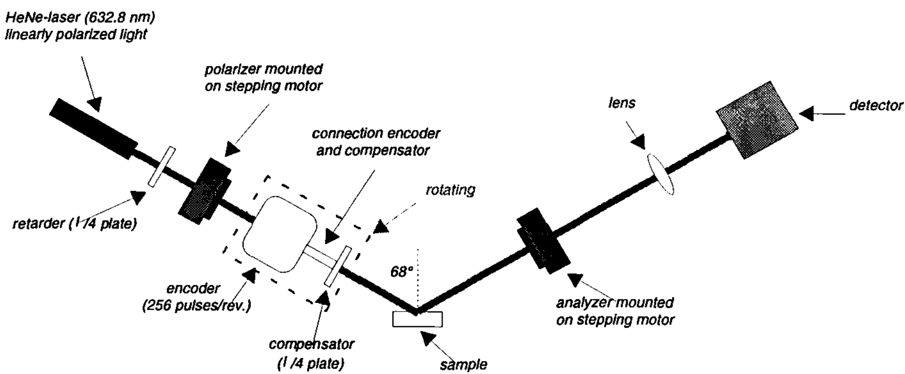

Figure 3.9: Setup for ellipsometry

Chapter 4

Argon-nitrogen plasmas

To study the influence of the injection of carbon in argon-nitrogen plasmas, first the argon nitrogen plasmas have been examined. In this chapter the results on these argon-nitrogen plasmas will be presented.

The argon-nitrogen plasmas are created in three different ways: by arc injection, by ring injection and by background injection. In the case of arc injection both argon and nitrogen are injected in the arc with a total flow of 100 scc/s, but with varying concentrations of nitrogen (0, 1, 2, 5, 10 and 20% of the total flow). In the case of ring injection argon is injected in the arc and nitrogen is admixed downstream via the ring. The total flow and the concentration of nitrogen are kept the same as in the experiments with arc injection. In the case of background injection, argon-nitrogen mixtures with a constant nitrogen flow of 5 scc/s are injected in the arc, and additional nitrogen is injected in the background of the vessel. Again the total flow is kept constant (100 scc/s). The amount of nitrogen injected in the background of the vessel is varied between 0, 5, 10 and 15 scc/s. In all three modes also the electrical current through the arc is varied: 48, 75 and 87 A. The settings for all three injection modes are listed in table 4.1.

The plasmas created in these ways are investigated with a Langmuir probe (§3.1). With the probe the electron temperatures and the electron densities of the different plasmas are determined. For arc injection and ring injection the distance between the arc and the probe is varied (30, 20, 10 and 5 cm) to determine the electron density and temperature as

Table 4.1: Settings of the argon-nitrogen plasmas.

	arc injection	ring injection	background injection
Total flow (scc/s)	100	100	100
N_2 flow (scc/s)	0; 1; 2; 5; 10; 15; 20	0; 1; 2; 5; 10; 15; 20	5; 10; 15; 20
N_2 injection	arc	ring	vessel and 5 scc/s in arc
I_{arc} (A)	48; 75; 87	48; 75; 87	48; 75; 87

a function of the distance from the nozzle. In §4.2 the differences in the electron densities of the different plasmas will be compared. The electron densities are also compared with a theoretical model (§4.1). In §4.3, the influence of the different plasmas on the electron temperature will be discussed.

Plasmas created by arc injection are also examined with optical emission spectroscopy (§3.2). With this method the rotational and vibrational temperatures of the first negative system (N_2^+) of nitrogen and the intensities of the emission of several nitrogen species are determined for plasmas of different compositions. The emission spectra will be discussed in §4.4. In §4.5, the rotational and vibrational temperatures for plasmas containing 5, 10, 15 and 20% nitrogen are compared.

4.1 Model for argon-nitrogen plasmas

A theoretical model [10] has been used to calculate the electron density and the densities of the different ions present in an expanding argon-nitrogen plasma at a given position in the vessel. These densities are calculated as a function of the nitrogen concentration in the flow through the arc. The electron and ion densities computed with this model will be compared with experimental values in §4.2.

To calculate the densities at a given position, first the densities of the different particles coming out of the arc has to be known. Because of the high temperatures inside the arc ($T_h \approx T_e \approx 1$ eV) the nitrogen molecules will be dissiocated and the only ions coming out of the arc will be the atomic ions Ar^+ and N^+. Assuming Partial Local Thermodynamic Equilibrium in the arc, the relative density of these ions can be calculated by the Saha equation [11]:

$$\frac{n_{N^+}}{n_{Ar^+}} = \frac{g(N^+)g(Ar)2N_{2flow}}{g(N)g(Ar^+)Ar_{flow}} \exp(\frac{E_{Ar^+} - E_{N^+}}{T_e}) \tag{4.1}$$

with n_{N^+} the density of N^+, n_{Ar^+} the density of Ar^+, $g(Ar)$ the statistical weight of the argon atom, $g(Ar^+)$ the statistical weight of the argon ion, $g(N)$ the statistical weight of the nitrogen atom $g(N^+)$ the statistical weight of the nitrogen ion, E_{Ar} the ionization energy for argon (15.76 eV) and E_N the ionization energy for nitrogen (14.53 eV). The statistical weights at 1 eV are 1, 5.7, 5.1 and 9.8, respectively [45]. In figure 4.1, the relative density of Ar^+ and N^+ as calculated from Eq.4.1, are given as a function of the percentage of nitrogen flow through the arc for electron temperatures inside the arc of 1 eV and 1.1 eV.

The plasma coming out of the arc expands into a vessel, where neutral argon and molecular nitrogen, which is formed on the walls, are present. The nitrogen molecules may be in an excited state, since the binding energy which is released during association, is partly used to excite the desorbing N_2 molecules. The total particle density in the vessel is calculated from the relation $pV = nkT$, with p the pressure inside the vessel during the experiments (25 Pa) and T the temperature of the neutrals (500 - 2000 K). The argon neutral and molecular nitrogen densities are given by their relative flows times the total particle density and are assumed to be homogeneously distributed in the vessel.

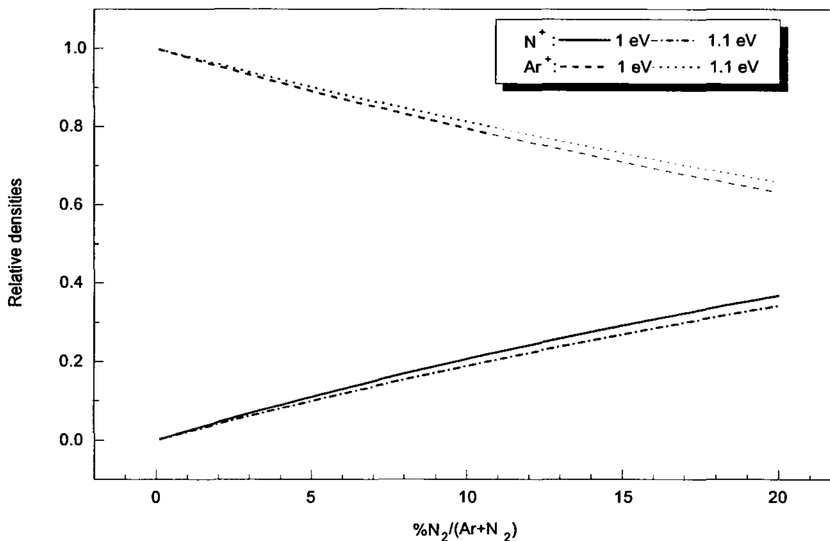

Figure 4.1: Relative density of Ar^+ and N^+ as a function of the percentage of nitrogen flow through the arc, calculated at electron temperatures of 1 eV and 1.1 eV.

Inside the vessel reactions between the different particles may occur, which change the densities of the different particles. The three reactions considered in this model are[1]:

$$Ar^+ + N_2 \rightarrow Ar + N_2^+ \ , k_1 \tag{4.2}$$

$$N^+ + N_2^* \rightarrow N + N_2^+ \ , k_2 \tag{4.3}$$

$$N_2^+ + e^- \rightarrow N^* + N \ , k_3 \tag{4.4}$$

Reactions 4.2 and 4.3 will reduce the amount of Ar^+ and N^+ ions while N_2^+ ions are produced, reaction 4.4 will reduce the amount of electrons and N_2^+ ions. The total of these three equations gives an effective loss of ions and electrons.

The reaction rates k_1, k_2 and k_3, depend on the electron temperature. However, the temperature is assumed to be independent of the position in the plasma, so the three reaction rates are assumed to be constant during the expansion. At 0.2 eV, the three reaction rates k_1, k_2 and k_3, are 7×10^{-17} m^3/s, 1×10^{-16} m^3/s and 10^{-13} m^3/s, respectively [10].

Inside the plasma, also other reactions may occur, (i.e. $Ar^+ + e^- + e^- \rightarrow Ar + e^-$). However, this reaction is a three particles reaction and the reaction rate is very slow (10^{-36} m^6/s [10]), and is therefore neglected in this model.

Reactions 4.2 and 4.4 are exothermal, reaction 4.3 becomes exothermal when the excitation energy of N_2^* is larger than 1 eV. In the case of an energy distribution with an average of 0.5 eV, only 13.5% of the nitrogen is excited to a level with a total energy larger than 1 eV. To account for the fact that the N_2^* concentration is lower than the total N_2 concentration, a lower reaction rate k_2 should be used in the model.

In this model, the diffusion of the different argon-nitrogen plasmas is assumed to be the same. Also the total amount of ions coming out of the arc, is assumed to be the same for

[1]particles denoted with * stand for excited particles

all plasmas. By taking the total ion density at every position, the same as the ion density of a pure argon plasma (which is known from experiments), the diffusion can be left out of this model and the model becomes 1-dimensional.

The final step in the model, is the calculation of changes in density of the different ions within the distance needed to reach the given position. These densities are computed from the starting densities, the densities of the neutrals and the rates of the three reactions. In order to compute the densities, the three reactions are put into differential forms. Because the downward velocity, v_d, of the particles is assumed to be constant, the differential equations can be given by:

$$\frac{\partial n_{Ar^+}}{\partial z} = -n_{Ar^+} n_{N_2} \frac{1}{v_d} k_1 \quad (4.5)$$

$$\frac{\partial n_{N^+}}{\partial z} = -n_{N^+} n_{N_2} \frac{1}{v_d} k_2 \quad (4.6)$$

$$\frac{\partial n_{N_2^+}}{\partial z} = n_{Ar^+} n_{N_2} \frac{1}{v_d} k_1 + n_{N^+} n_{N_2} \frac{1}{v_d} k_2 - n_e n_{N_2^+} \frac{1}{v_d} k_3 \quad (4.7)$$

where $n_e = n_{Ar^+} + n_{N^+} + n_{N_2^+}$ is the electron density, which follows from quasi-neutrality. These differential equations are solved numerically.

The parameters which can be varied in this program, are the measuring position (5 - 65 cm), the velocity v_d of the plasma (500 - 1000 m/s), the density of the neutrals inside the vessel, the electron density coming out of the arc (approximately 10^{20} m^{-3}) and the rates for reactions 4.2, 4.3 and 4.4.

4.2 Electron densities

The electron density for arc injection as a function of the concentration of nitrogen is shown in figure 4.2. From this figure it is clear that the electron density is higher for higher currents through the arc. This is caused by the fact that the degree of ionization of the gas is higher for higher arc power. In figure 4.3 the electron density as a function of the concentration of nitrogen is shown for arc injection, ring injection and background injection. These figures also show that in all cases the electron density decreases with increasing nitrogen concentration. The electron densities in pure argon plasmas lie between 18×10^{18} m^{-3} and 32×10^{18} m^{-3}, depending on the arc current, while the values for plasmas containing 20% nitrogen lie between 2×10^{18} m^{-3} and 7×10^{18} m^{-3}.

To understand these results, it is necessary to examine the particles present in the plasma and the reactions that can occur between them. In the case of ring injection the only ion coming out of the arc is the argon ion and the nitrogen is admixed downstream. In the case of arc injection or background injection (where we always have 5 scc/s nitrogen in the arc, see table 4.1), also nitrogen ions will come out of the arc. The relative densities of the Ar^+ and the N^+ ions can be calculated using Eq.4.1. The plasma expands into a vessel, where neutral argon and molecular nitrogen, which is formed on the walls, are

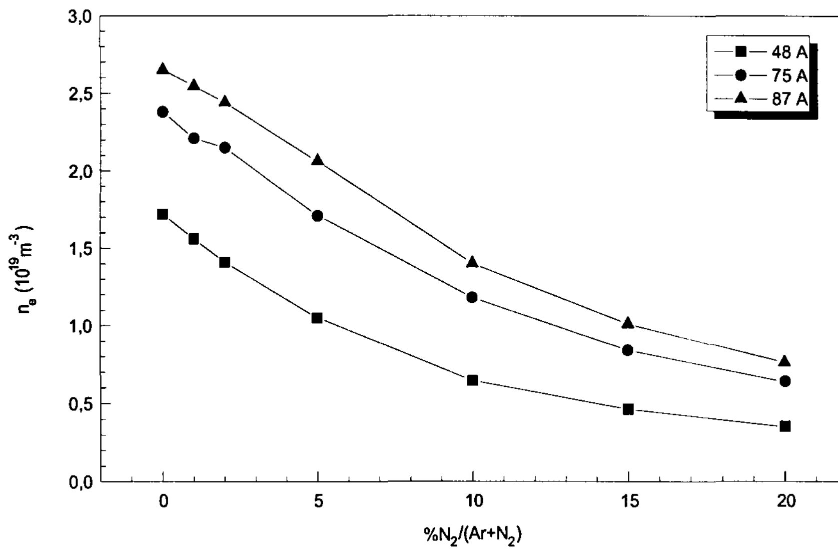

Figure 4.2: Electron density at 20 cm from the nozzle as a function of nitrogen concentration for arc injection. The electrical current through the arc is 48 A, 75 A and 87 A.

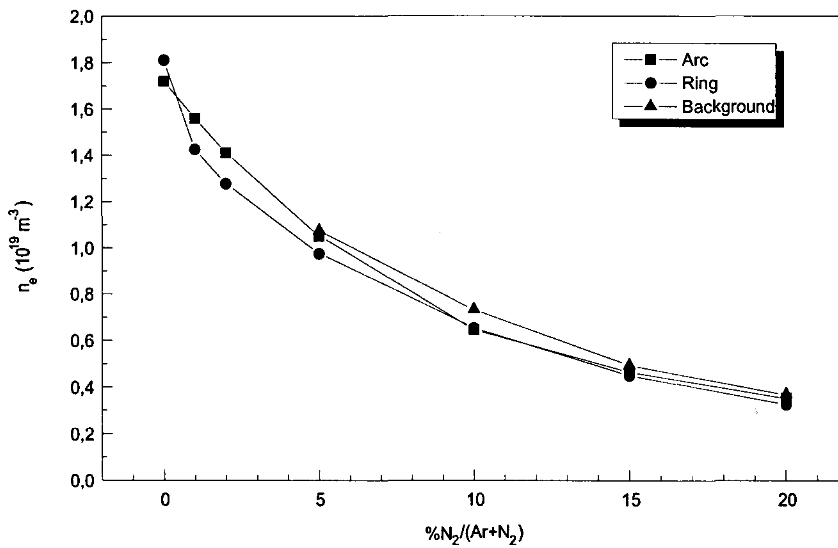

Figure 4.3: Electron density at 20 cm from the nozzle as a function of nitrogen concentration for arc injection, ring injection and background injection. The electrical current through the arc is 48 A.

present. Here the reactions 4.2, 4.3 and 4.4, as described in §4.1, may occur. These three reactions show that admixing nitrogen, leads to the loss of ions and electrons.

The different injection methods result in practically the same electron densities (see figure 4.3). This means that the loss of electrons is the same for all three injection methods. Therefore, the value for $n_e n_{N_2^+} k_3$, has to be the same for the three methods. Because the electron density is the same for the three methods, the value for $n_{N_2^+} k_3$, has to be the same. The sum of the amount of Ar^+ and N^+ coming out of the arc is almost the same for the three injection methods, so in order to form the same amount of N_2^+, the values for $n_{N_2} k_1$ and $n_{N_2^*} k_2$ should have the same order of magnitude. However, the value for $n_{N_2^*} k_2$ taken in the simulation to obtain good agreement with the experiments for the arc injection, is one order of magnitude lower than the value for $n_{N_2} k_1$, as will be seen below. When the reaction rates k_1, k_2 and k_3 would be the same for all three methods, this would result in a different electron densities for the different methods, as can be seen in the simulations in figure 4.5. When nitrogen is injected in the ring or the background, the values of the reaction rates k_1, k_2 and k_3 apparently differ from the values when nitrogen is injected in the arc.

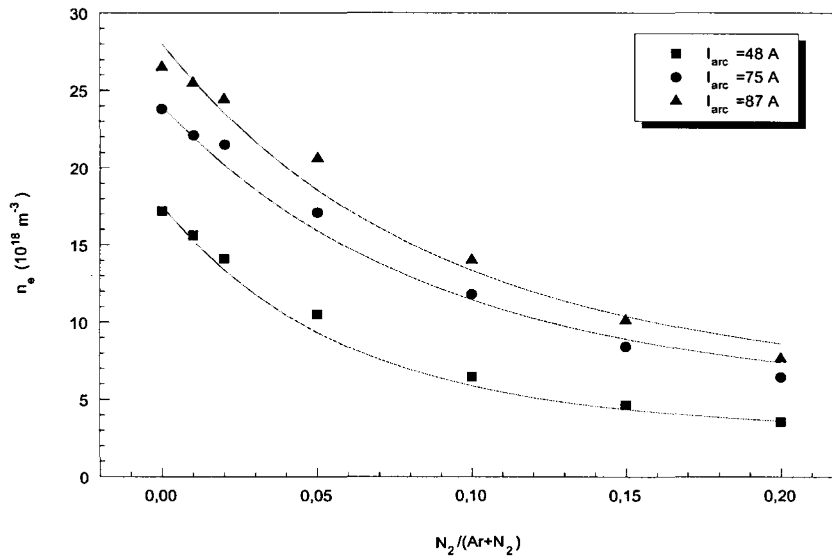

Figure 4.4: Measured electron densities (symbols) in the case of arc injection with an electrical current through the arc of 48 A, 75 A and 87 A at 20 cm from the nozzle and the values calculated with the theoretical model (lines).

The results of the experiments are also compared with a model (see §4.1) in which the electron density at a given position downstream is calculated as a function of the relative flow of the gases in the arc. The results of this model for arc injection, are given in figure 4.4, and for arc, ring and background injection in figure 4.5. To obtain good agreement with the experiments, in the simulations of arc injection, the values 7×10^{-17} m^3/s, 1×10^{-17} m^3/s and 10^{-13} m^3/s had to be taken for the rates of reactions 4.2, 4.3 and 4.4, the value 1000 m/s for the drift velocity, and the value 1.0×10^{21} m^{-3} for the neutral

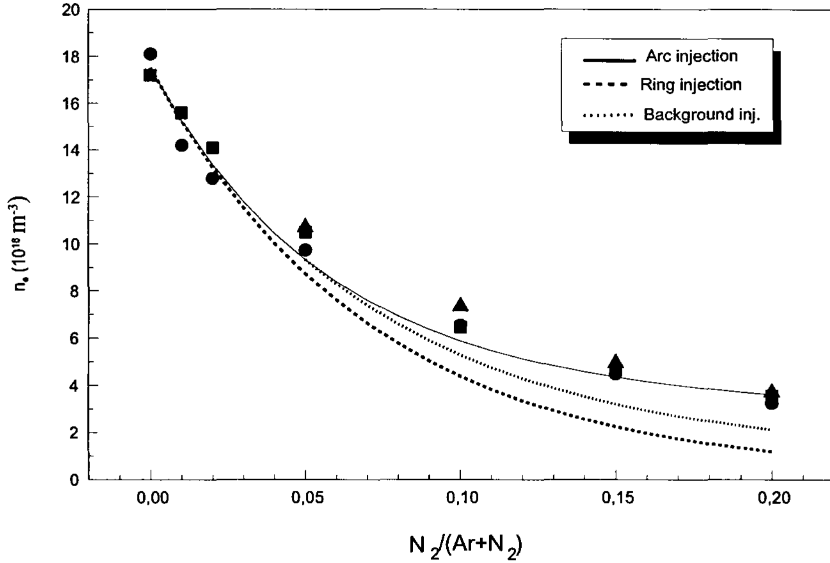

Figure 4.5: Measured electron densities at 20 cm from the nozzle (symbols) and the values calculated with the theoretical model for arc injection (solid line), ring injection (dashed line) and background injection (dotted line).

particle density in the vessel. The rate for reaction 4.3 used in the model is lower than the value in literature (1×10^{-16} m^3/s [10]), because in the model the total N_2 concentration is taken to calculate the production of N_2^+ by reaction 4.3, instead of the concentration of N_2^*. To account for the fact that the N_2^* concentration is lower than the total N_2 concentration, this lower reaction rate is used (see §4.1). The neutral particle density used in the simulations, is half the value which is calculated from the relation $pV = nkT$, with a gas temperature of approximately 1000 K. The amount of argon neutrals in the vessel, has no effect on the electron density, because it does not contribute to any reaction. The amount of neutral nitrogen molecules in the vessel, however, influences the formation of N_2^+ by reactions 4.2 and 4.3. The smaller value for the amount of nitrogen in the vessel, used in the simulation, will thus slow down the formation of N_2^+, and thus the decrease of the electron density by reaction 4.4. A possible explanation for the lower particle density in the simulation than the particle density calculated from a gas temperature of 1000 K in the plasma, is that the gas temperature is not 1000 K but 2000 K, leading to half the nitrogen concentration. Another possible explanation for the lower value for the nitrogen concentration is, that in the experiments not all nitrogen molecules, which are formed on the wall of the vessel, can reach the expansion axis again, where the probe measurements are performed, because they already react on the outside of the plasma. This will result in a lower concentration of N_2 on the expansion axis, than expected at that temperature. This assumption is supported by emission measurements of the intensity of N_2^+ as a function of the radial position (figure 4.6). In this figure one can see that the emission of N_2^+, which may be formed in reaction 4.3, is much smaller in the center of the plasma than at the outside.

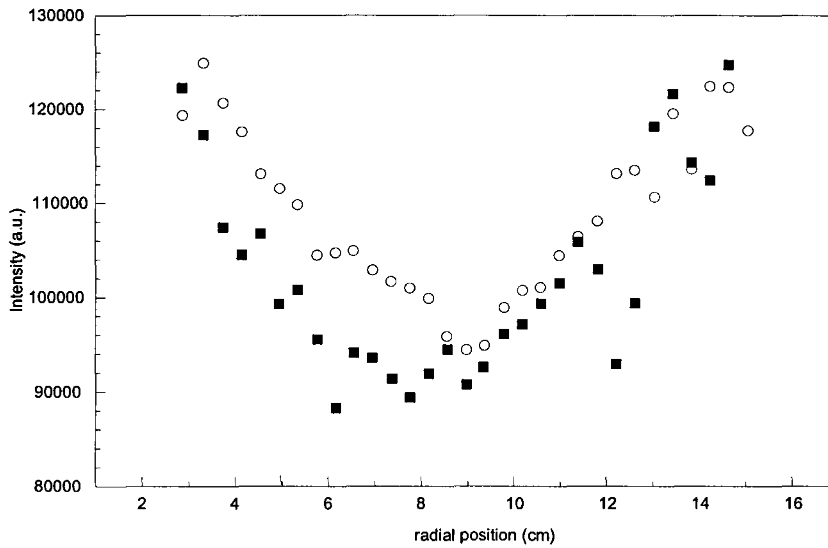

Figure 4.6: Emission measurements of the intensity of N_2^+ as a function of the radial position. The total gas flow is 100 scc/s. Measurements of G.J.H. Brussaard.

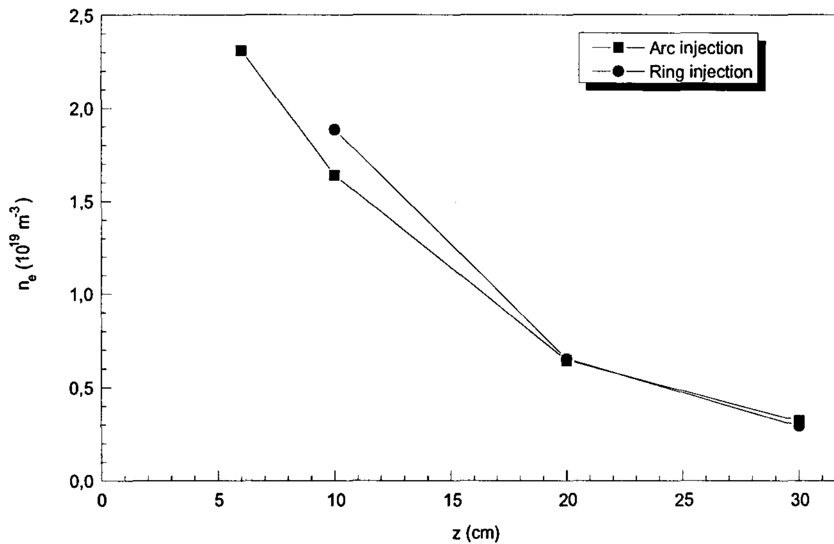

Figure 4.7: Electron density as a function of the distance from the nozzle for arc injection and ring injection. The nitrogen flow is 10% of the total flow, the electrical current through the arc is 48 A.

In figure 4.7 the electron density as a function of the distance from the nozzle is shown for arc injection and ring injection. This figure shows that the electron density decreases with the distance from the arc. This can be explained by charge exchange reactions 4.2 and 4.3 followed by dissociative recombination reaction 4.4. The molecular nitrogen ions produced upstream, recombine (reaction 4.4), leading to the loss of an ion and an electron. This process will also take place downstream, but due to the lower ion and electron densities here, the three reactions 4.2 , 4.3 and 4.4, will slow down. The production and recombination of N_2^+ will slow down, and as a consequence the decrease in the electron density.

4.3 Electron temperatures

The electron temperatures of these plasmas are also determined. The electron temperature as a function of the relative nitrogen flow for arc injection is shown in figure 4.8 The electron temperatures as a function of the nitrogen concentration for arc injection, ring injection and background injection are given in figure 4.9.

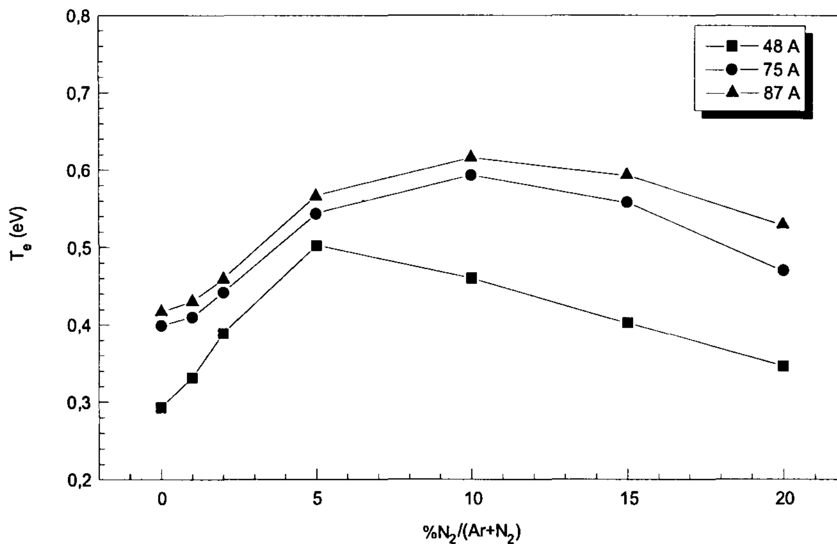

Figure 4.8: Electron temperature at 20 cm from the nozzle as a function of nitrogen concentration for arc injection. The electrical current through the arc is 48 A, 75 A and 87 A.

When nitrogen is injected in the arc we can see from figure 4.8 that first the electron temperature increases with increasing nitrogen concentration, then the electron temperature reaches a maximum and a further increase of the nitrogen concentration causes a decrease of the electron temperature. The electron temperature in the case of pure argon plasmas lies between 0.28 and 0.41 eV, depending on the arc current. The increase of electron temperature with increasing arc current is also seen in other studies [44]. The

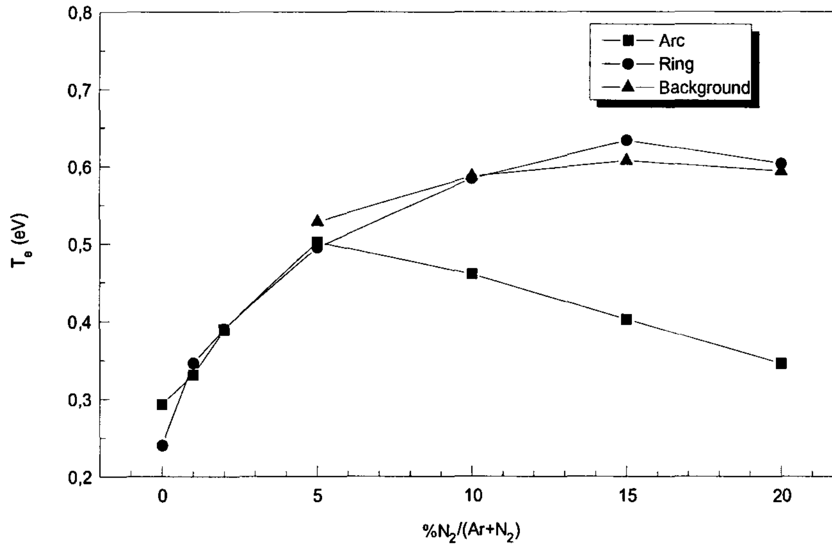

Figure 4.9: Electron temperature at 20 cm from the nozzle as a function of nitrogen concentration for arc injection, ring injection and background injection. The electrical current through the arc is 48 A.

maximum electron temperature occurs at a nitrogen concentration between 5% and 10% and lies between 0.50 and 0.61 eV, depending on the electrical current through the arc. A higher current leads to a higher electron temperature and also to a shift of the maximum to a higher nitrogen concentration.

A possible explanation for the increase of the electron temperature on the addition of nitrogen in the arc, is excited nitrogen species (N_2^*, N_2^{+*}, N^*) having 'super elastic' collisions with the electrons. In these collisions they transfer their excitation energy to the electrons. Especially metastable[2] species have a mean optical lifetime (10^{-3} s - 1 s, compared to normally 10^{-8} s [14]) which is long enough for these collisions to occur. One of the possible reactions could be:

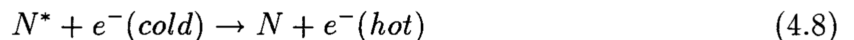

$$N^* + e^-(cold) \rightarrow N + e^-(hot) \qquad (4.8)$$

N_2^* may be formed by recombination of nitrogen atoms at the vessel walls or by excitation exchange with Ar^*, N^* is formed by reaction 4.4 and N_2^{+*} may be formed by reaction 4.3 when the excitation energy of the N_2^* is higher than the 1.05 eV needed for this reaction. The concentrations of these three excited nitrogen species are related to the formation of N_2^+, because the increase of N_2^+ will result in an increase of N^* by reaction 4.4 and this will also result in an increase of formation of N_2^* on the walls of the vessel and thus on the formation of N_2^{+*} by reaction 4.3.

Another explanation is that the recombination reaction 4.4 mainly favors low energy electrons, due to the $T_e^{-1/2}$ dependence of k_3 [49]:

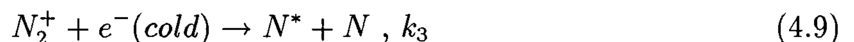

$$N_2^+ + e^-(cold) \rightarrow N^* + N \ , \ k_3 \qquad (4.9)$$

[2]excited species for which no allowed transitions to any lower state can occur

This reaction mainly leads to the loss of the low energy electrons, leaving behind the electrons with a higher energy. Eventually, this leads to an increase of the average electron temperature by electron-electron relaxation collisions.

In both cases, i.e. heating of the electrons by super elastic collisions and the recombination mainly taking place with low energy electrons, the heating of the electron temperature is related to the N_2^+ concentration. So, to get a better insight into the behaviour of the electron temperature, we have to look again at Eq. 4.1 and the reactions 4.2, 4.3 and 4.4. Admixture of nitrogen in the arc causes an increase of the N_2 and the N^+ concentrations and a decrease of the Ar^+ concentration. The relative densities of Ar^+ and N^+ are calculated with equation 4.1. At first the increase of N_2 will contribute to the increase of N_2^+ by reactions 4.2 and 4.3. Also the increase of N^+ will cause an increase of N_2^+. When the concentration of nitrogen increases, a point will be reached where the amount of Ar^+ becomes the dominant factor in reaction 4.2. An increase of nitrogen, resulting in a decrease of Ar^+, will then lead to a decrease of N_2^+ formed by reaction 4.2. This decrease in the formation of N_2^+ by reaction 4.2 might only partially be compensated by the increase of N_2^+ formed by reaction 4.3, because this reaction depends also on the amount of N_2^* and this might be low on the expansion axis, as is discussed before. The amount of N_2^+ will thus first increase with increasing nitrogen concentration, reach a maximum and then it will decrease with increasing nitrogen concentration. This effect can also be seen in figure 4.10, where the amount of N_2^+ as a function of the nitrogen concentration, calculated by the theoretical model, is given. As discussed before, the electron temperature will be related to the N_2^+ concentration.

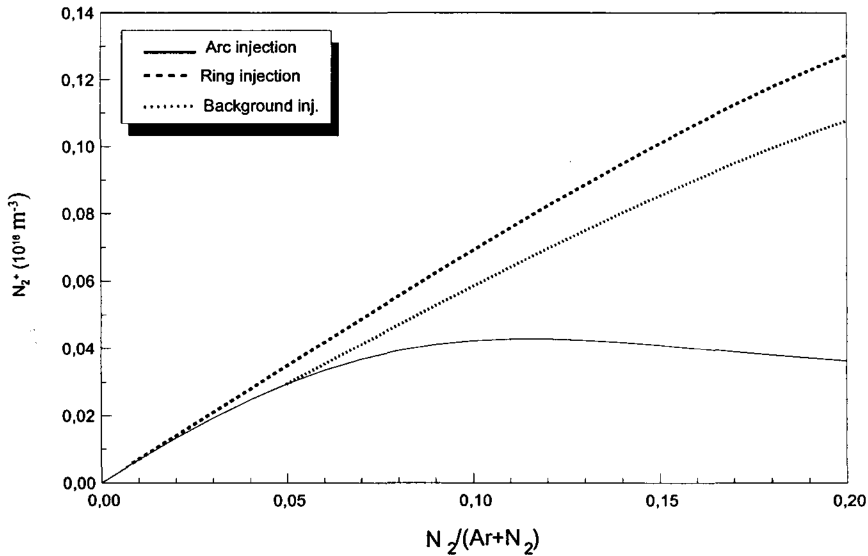

Figure 4.10: Concentration of N_2^+ as a function of the nitrogen concentration, for arc, ring and background injection, as calculated with a theoretical model.

The effect that higher arc currents lead to a maximum of the electron temperature at a higher nitrogen concentration (see figure 4.8), can be explained by the higher ionization degree at higher arc currents. Because of this higher ionization degree, the decrease in the formation of N_2^+ at the expansion axis caused by the decrease of Ar^+ will start at a higher nitrogen concentration. Another possibility would be that the electron temperature in the arc increases with increasing nitrogen concentration, leading to a shift in the relative concentrations of Ar^+ and N^+ to a higher Ar^+. At a nitrogen concentration of 20%, the relative amount of Ar^+ increases from 63%, at an electron temperature of 1 eV in the arc, to 65%, at an electron temperature of 1.1 eV in the arc (see figure 4.1). So this effect is too low to explain the observed shift of the maximum in the electron temperature.

When the nitrogen is injected in the ring, we can see from figure 4.9 that the electron temperature (0.27 eV in the case of a pure argon plasma) at first increases with increasing nitrogen concentration, reaches a maximum (0.63 eV) around 15% and then only decreases with increasing nitrogen concentration. The increase of the electron temperature can be explained in the same way as for arc injection. The amount of N_2^+ increases with increasing nitrogen concentration, except now the only way it is formed is by reaction 4.2, because there is no N^+. The increase of the N_2^+ concentration leads to a higher electron temperature, as is discussed above. In the case of ring injection the electron temperature still increases with increasing nitrogen concentration while in the case of arc injection the electron temperature decreases. Because only argon is injected in the arc, the amount of Ar^+ does not decrease significantly with increasing nitrogen concentration, as was the case for arc injection (see figure 4.1). Furthermore, the total amount of argon ions will be higher when nitrogen is injected in the ring. The higher amount of Ar^+ causes the production of N_2^+ by reaction 4.2 still to increase, which leads to an increase of the electron temperature. When the concentration of nitrogen is increased further, again a point will be reached where the amount of Ar^+ becomes the dominant factor in reaction 4.2. A further increase of the amount of nitrogen will not lead to a further increase of the amount of N_2^+ and the electron temperature will saturate. Because the total flow is kept constant, the argon flow through the arc is decreased when the nitrogen concentration is increased. This may lead to a decrease of the amount of Ar^+ with increasing nitrogen concentration. As a result, the amount of N_2^+ might slightly decrease and thus also the electron temperature, when the nitrogen concentration is increased even further.

When the nitrogen is injected in the background of the vessel, we can see from figure 4.9 that increasing the nitrogen concentration has the same effect on the electron temperature as in the case of ring injection. In the case of background injection also a nitrogen flow of 5 scc/s is injected in the arc. This causes a decrease of Ar^+ of 11% - 13%, depending on the argon flow, compared to the ring injection. This should cause the maximum in the electron temperature to be a little lower and at a lower nitrogen concentration. These effects are however so small (0.05 eV lower, respectively 1% lower), that they can not be observed in figure 4.9.

In §4.2, it was seen that the values k_1, k_2 and k_3 of the reaction rates for ring injection or background injection, may differ from the values for arc injection. Because the

reaction rates depend on the electron temperature, this difference may be explained by the observed difference in the electron temperature for the three injection modes (see figure 4.9).

In figure 4.11 the electron temperature as a function of the distance from the nozzle is shown for the case of arc injection and ring injection. The electron temperature tends to increase with the distance. This can be explained by the following mechanism. N_2^+ formed in the beginning will recombine, resulting in an increase of the electron temperature upstream, either by super elastic collisions with metastable species, or by the $T_e^{-1/2}$ dependence on the recombination rate k_3. Downstream, again N_2^+ is formed by reactions 4.2 and 4.3. This N_2^+ will also recombine, resulting in a further increase of the electron temperature downstream. For distances larger than 10 cm the electron temperature only slightly increases with increasing distance. The electron density and ion density at this position are low, causing the reactions 4.2, 4.3 and 4.4 to be slow. The formation and recombination of N_2^+ will thus be slow, resulting in an increase of the electron temperature which slows down with increasing distance from the arc. The difference in the temperature for arc injection and ring injection is caused by the nitrogen flow dependence of the electron temperature (see figure 4.9).

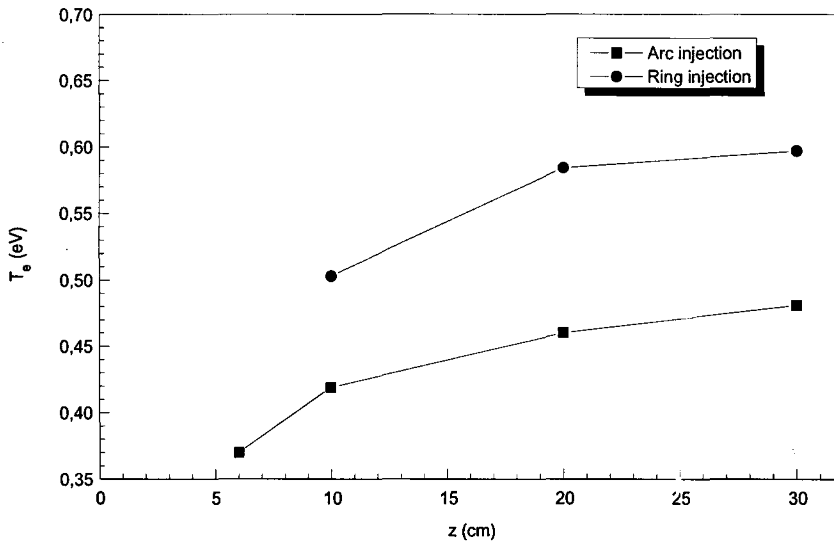

Figure 4.11: Electron temperature as a function of the distance from the nozzle for arc injection and ring injection. The concentration of nitrogen is 10%.

4.4 Emission spectroscopy

The argon-nitrogen plasmas created by arc injection are also investigated with optical emission spectroscopy. With this technique, the intensities of emission lines and the bandheads of some nitrogen species are determined as a function of the nitrogen concentration. When measured under the same optical conditions, these intensities give us an indication of the relative amount of particles present in an excited state. The results of these intensity measurements for the bandheads at 375.54 nm (N_2: $C^3\Pi \rightarrow B^3\Pi$, see figure 3.4), at 391.44 nm (N_2^+: $B^2\Sigma \rightarrow X^2\Sigma$) and the N-line at 409.99 nm and are given in figure 4.12.

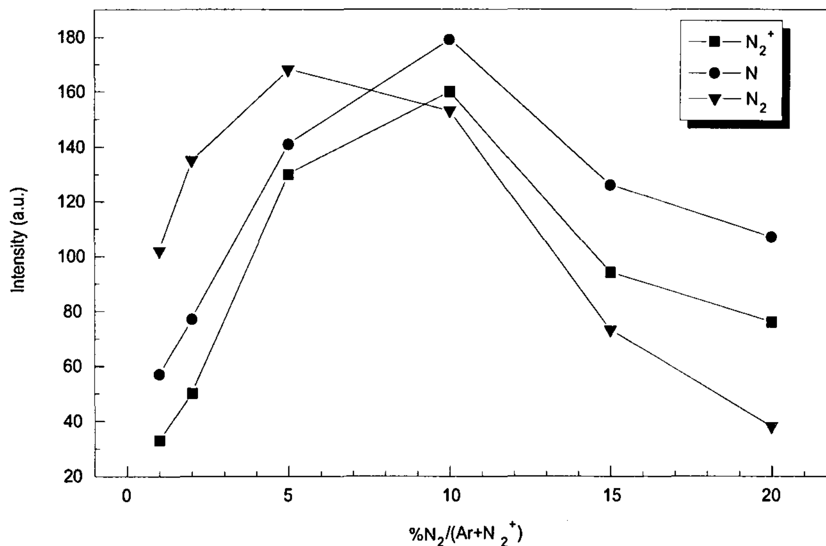

Figure 4.12: The intensity of different lines and bandheads emitted by nitrogen species, measured 32 cm from the nozzle, as a function of the nitrogen concentration. The arc current is 48 A.

We can see from this figure that when the amount of nitrogen injected in the arc increases, at first the intensity of all three bandheads and lines increases, to reach a maximum. A further increase of the nitrogen concentration causes a decrease in the intensity of all three lines. The maxima lie between 5% and 10%.

If we compare figure 4.12 with figure 4.10 in which the amount of N_2^+ as a function of the nitrogen concentration is depicted, we see a high degree of resemblance. The concentrations of the excited nitrogen species are partially related to the concentration of N_2^+, because N_2^{+*} may be formed by reaction 4.3, N^* by reaction 4.4 and N_2^* may be formed by recombination of nitrogen atoms (formed by reaction 4.4) at the vessel walls, or by excitation transfer between Ar^* and N_2. If we compare figure 4.12 with figure 4.8 in which the electron temperature is presented as a function of the nitrogen concentration, again we can see a high degree of resemblance. This resemblance may support the assumption that these excited nitrogen species could be responsible for the heating of the electrons by super elastic collisions. However, this resemblance may also indicate that higher electron temperatures cause more particles to be excited.

4.5 Rotational and vibrational temperatures

Outside the arc the plasma is recombining ($\frac{dn_e}{dt} \neq 0$). In such a non-equilibrium system the energies of the electrons and of the rotational, vibrational and translational state of the molecules may differ from each other. The vibrational and rotational levels of a molecule can be excited by the electrons. Only at higher energies the translation modes of the molecule will get involved.

To examine the difference with an equilibrium system, the energy exchange between electrons and the rotational and vibrational energies of nitrogen have been investigated. For this, optical emission spectra of the argon-nitrogen plasmas have been recorded in the DEPO I laboratory and from these data, E. Aldea[3] and G. Dinescu[3] have determined with a computer simulation procedure [16], the vibrational and rotational temperatures of the argon-nitrogen plasmas. These temperatures have been determined from the $B^2\Sigma \rightarrow X^2\Sigma$ (see figure 3.4) transition of N_2^+. The results are shown in figures 4.13 and 4.14, respectively.

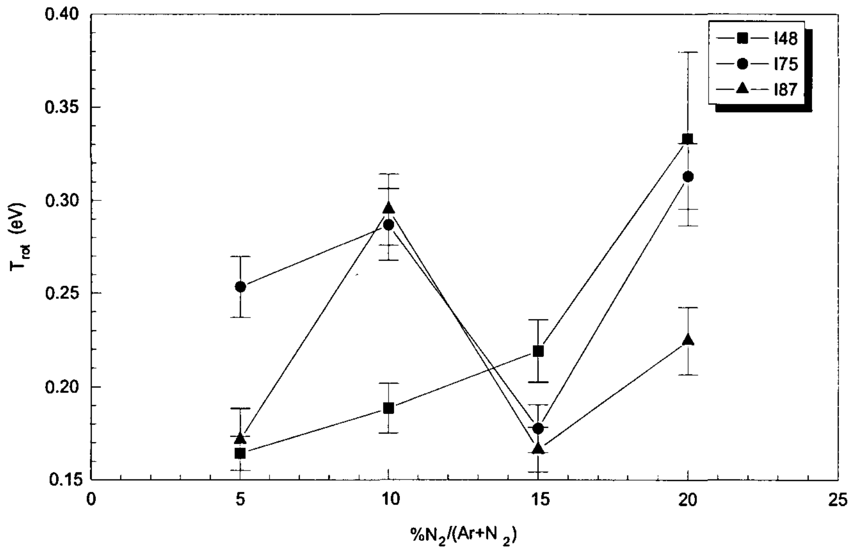

Figure 4.13: The rotational temperature of N_2^+ $B^2\Sigma \rightarrow X^2\Sigma$, as derived from the simulations of the measured spectra 32 cm from the nozzle, as function of the nitrogen concentration. The arc currents are 48, 75 and 87 A, the entrance slit of the monochromator was 50 μm and the integration time 0.5 s.

In figure 4.13 it can be seen that the rotational temperature of the different plasmas varies between 0.16 eV and 0.34 eV and has no clear relationship with the composition of the plasma. The average rotational temperature is 0.25 eV and this is close to the electron temperature measured in pure argon plasmas (see §4.3).

[3]Institute of Physics and Technology of Radiation Devices, Low Temperature Plasma Departement, Bucharest, Rumania

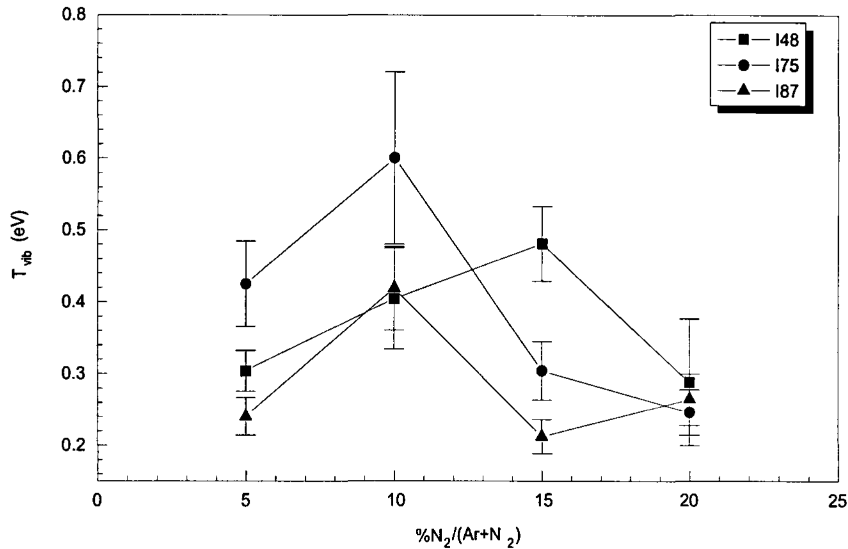

Figure 4.14: The vibrational temperature of the nitrogen, as derived from the simulations of the measured spectra of the first negative system of nitrogen, measured 32 cm from the nozzle, as function of the nitrogen concentration. The arc currents are 48, 75 and 87 A.

The vibrational temperature varies between 0.22 eV and 0.60 eV. It first increases with the nitrogen concentration, reaches a maximum around a nitrogen concentration of 10%, and then decreases. If we compare the vibrational temperature with the electron temperature (figure 4.8), we see that they have similar dependencies on the nitrogen concentration. Both first increase with increasing nitrogen concentration, to reach a maximum around a nitrogen concentration of 10%. A further increase of the nitrogen concentration causes in both cases a decrease. If we compare the values of the vibrational temperature and the electron temperature, we see that they are in good agreement with each other.

Apparently the exchange between the electron energy and the vibrational energy is pretty good. The exchange between these energies and the rotational energies however, seems hardly to take place. If the exchange between the rotational energy and the translational energy of the neutrals is good, the gas temperature would be 0.25 eV, which would support the assumption that the lower density of the neutral particles as derived from the model in §4.2, can be explained by a two times higher gas temperature (i.e. 2000 K instead of 1000 K).

Chapter 5

The evaporator

The first method used to inject hydrogen-free carbon in plasmas is with the evaporator. With this evaporator fullerene and graphite have been evaporated and injected in the plasma with a carrier gas (argon). The plasmas with fullerene and graphite vapor have been studied with optical emission spectroscopy (§3.2). The setup of the evaporator and the different plasma settings, are described in §5.1.

In §5.3, the experiments with fullerene (C_{60}) will be discussed. With optical emission spectroscopy first the reaction products of the plasma and the vapor have been examined. From these reaction products, the possible reactions between the argon plasma and the fullerene vapor have been determined. The relative amount of the reaction products inside the plasma is also examined as a function of the temperature in the evaporator. This will be compared with the vapor pressure of fullerene, known from literature. Furthermore, the evaporation rate at a temperature of 750^0C is determined and is compared with the value, calculated as described in §5.2.

In §5.4, the results of the evaporation of graphite will be discussed. The reaction products of the plasma and the vapor have been examined with optical emission spectroscopy. The relative amount of the reaction products inside the plasma is also examined as a function of the temperature in the evaporator and will be discussed.

5.1 Setup of the evaporator

To inject carbon into the expanding plasma, an evaporatoı for C_{60} and graphite has been constructed. The evaporator can be connected to the vessel. By changing the temperature of the heater, the vapor pressure can be changed. In this way the amount of carbon injected in the plasma can be controlled. A schematic drawing of the evaporator is shown in figure 5.1.

To get hydrogen-free carbon inside the plasma, fullerene and graphite powder were used for evaporation. The powder is situated in the drum (1). This drum can be heated by a heating element of 500 W (2). To prevent heating by plasma radiation and to optimize the yield of the heating element a radiation shield (3) is put around the drum. The temperature

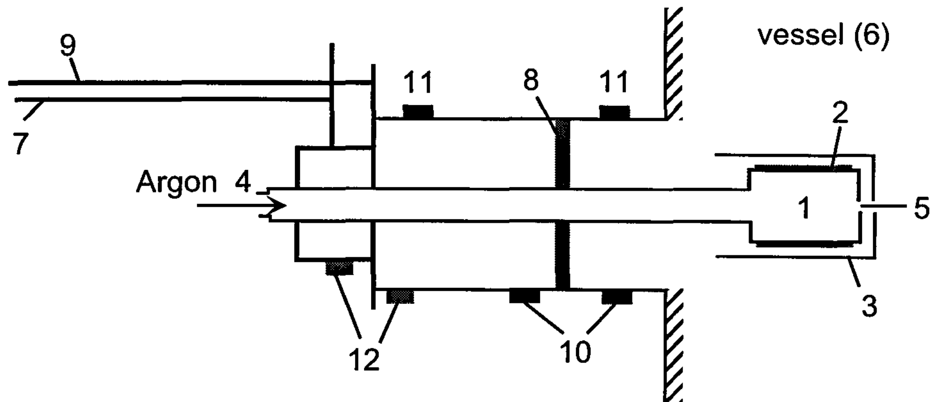

Figure 5.1: Schematic drawing of the evaporator. The numbers are explained in the text.

inside the drum can be measured with a chrome-aluminum thermocouple (Thermocoax, type K). To get the vapor inside the vessel a carrier gas (argon) flows from the gas inlet (4) through the drum and the hole (5) to the vessel (6). The argon flow can be regulated with a mass flow controller (Bronckhorst, type F- 201C-FA). The operation and the calibration of the flow controller are described in appendix A. To detach the evaporator from the vessel it can be shoved backwards with the arm (7) and the pneumatic valve (8) can be closed. To refill the drum with fullerene or graphite, the evaporator can be shoved further backward with another arm (9). The evaporator is water cooled (10: inlet, 11: outlet). The controlling of the temperature in the drum, the cooling water and the valve takes place with a separate PLC unit and is described in appendix B.

The settings of the different plasmas used during the experiments with the evaporator are listed in table 5.1 below.

Table 5.1: Settings used during the experiments with the evaporator.

	Ar+C_{60}	Ar+graphite
Ar flow in arc (scc/s)	25	25
Ar flow evaporator (scc/s)	10	7.5; 10
Temperature evaporator (^{0}C)	300-775	300-1030
I_{arc} (A)	30	35
p_{vessel} (mbar)	0.15	0.15
distance arc-evaporator (cm)	5	5

5.2 Evaporation rate of C_{60}

The evaporation rate is expressed in weight loss (dw) per time. The relation between the evaporation rate (dw/dt) and the saturated vapor pressure (p_s) is given by the equation [8]:

$$p_s = \frac{1}{A}\frac{dw}{dt}\sqrt{\frac{2\pi kT}{m}} \tag{5.1}$$

where A is the surface of the powder, k is the Boltzmann constant, T is the temperature and m the mass of the molecule. For the saturated vapor pressure of C_{60} Matsumoto et al. [9] derived from experiments the following formula:

$$p_s = p_0 \exp\left(-\frac{18899}{T}\right) \tag{5.2}$$

where p_0 is 81.28×10^3 atm.

Combining these two equations gives a relation between the evaporation rate, the surface from which C_{60} evaporates and the temperature:

$$\frac{dw}{dt} = p_0 A\sqrt{\frac{m_{C_{60}}}{2\pi kT}}\exp\left(-\frac{18899}{T}\right) = K_T A \tag{5.3}$$

where $K_T = p_0\sqrt{\frac{m_{C_{60}}}{2\pi kT}}\exp\left(-\frac{18899}{T}\right)$ depends on the temperature only.

The drum of the evaporator is a cylinder, so the area of C_{60} can be described by the configuration sketched in figure 5.2. For the surface of C_{60} the following approximation holds:

$$A = 2lR\sin\phi \tag{5.4}$$

The volume of C_{60} inside the drum can be expressed by:

$$V = lA_2 = lR^2(\phi - \cos\phi\sin\phi) = lR^2(\phi - \frac{1}{2}\sin 2\phi) \tag{5.5}$$

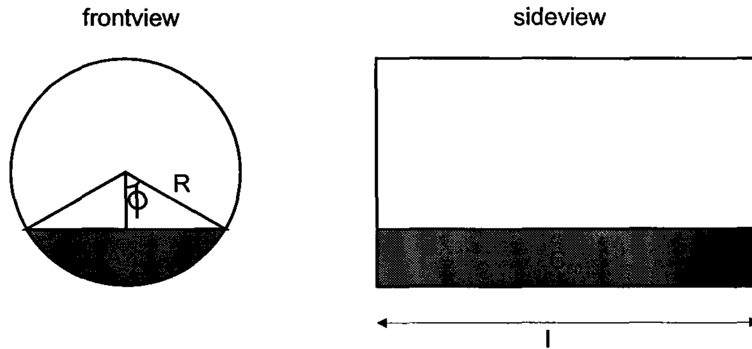

Figure 5.2: Schematic drawing of the drum of the evaporator

Because the powder lies on the wall of the cylinder, the angle ϕ and the surface of C_{60} change during the experiments. The change of ϕ is related to the evaporation rate by the formula:

$$\frac{dw}{dt} = -\rho\frac{dV}{dt} = -\rho l\frac{dA_2}{dt} = -\rho l(R^2 - R^2\cos 2\phi)\frac{d\phi}{dt} \tag{5.6}$$

where ρ is the specific mass of C_{60}. Combining this with equations 5.3 and 5.4 gives:

$$2lK_TR\sin\phi = -\rho lR^2(1-\cos 2\phi)\frac{d\phi}{dt} \tag{5.7}$$

From this equation it can be derived that the total time necessary to evaporate an amount of C_{60} is given by:

$$\int_{t=0}^{t_e} dt = -\frac{\rho R}{2K_T}\int_{\phi_0}^{0}\frac{1-\cos 2\phi}{\sin\phi}d\phi = -\frac{\rho R}{2K_T}\int_{\phi_0}^{0}2\sin\phi d\phi = \frac{\rho R}{K_T}(1-\cos\phi_0) \tag{5.8}$$

where t_e and ϕ_0 are the time when all the fullerene is evaporated and the angle at the beginning of the evaporation, respectively. The angle ϕ_0 can be calculated from the weight of C_{60} in the drum and eq. 5.5.

In experiments the evaporation rates will differ from the calculated rates, because the fullerene in the drum is a powder and it will lie on a heap instead of the neatly distribution sketched in figure 5.2. This will result in an increase of the evaporation surface, causing an increase of the evaporation rate.

5.3 Fullerene

Fullerene vapor has been injected in argon plasmas with the evaporator. Of such a plasma an optical emission wavelength scan has been made to investigate the particles present in the plasma. A wavelength scan of an argon plasma with fullerene vapor is shown in figure 5.3. In this spectrum the Swan transition bands of C_2 ($A^3\Pi \rightarrow X^3\Pi$) are clearly observed. The energy needed to excite the carbon dimer molecule to the $A^3\Pi$ level, is 2.48 eV. In this spectrum also an argon line can be observed.

From this spectrum it can be concluded that one of the fragmentation products of C_{60} in an argon plasma is C_2. This is in agreement with [40] and [42]. The fragmentation may take place by ionization of fullerene with electrons [42]:

$$C_{60} + e^- \rightarrow C_{60}^+ + 2e^- \tag{5.9}$$

followed by dissociation into C_2 and C_{58}^+. However, the ionization potential of C_{60} is 7.6 eV and in our case the energy of the electrons is approximately 0.2 eV, so the electron energy is too low for ionization of fullerene by reaction 5.9. In our case, a possible ionization reaction of fullerene may be the charge exchange reaction with argon:

$$Ar^+ + C_{60} \rightarrow Ar + C_{60}^+ \tag{5.10}$$

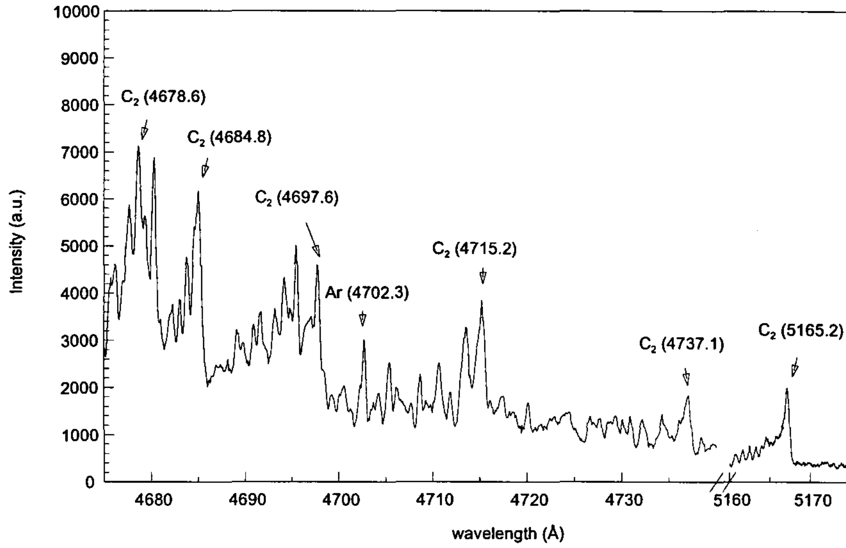

Figure 5.3: Emission spectrum of an argon plasma in which C_{60} vapor is injected. The argon flow through the arc is 25 scc/s and through the evaporator 10 scc/s. The arc current is 30 A, the temperature in the evaporator 750^0C, the integration time 0.5 s and the slit 50 μm.

The fullerene ion can decay by the following reactions [42]:

$$C_{60}^{+} \rightarrow C_{58}^{+} + C_2^* \quad (5.11)$$

$$C_{58}^{+} \rightarrow C_{56}^{+} + C_2^* \quad (5.12)$$

$$C_{56}^{+} \rightarrow C_{54}^{+} + C_2^* \quad (5.13)$$

The carbon dimer is assumed to get excited during the fragmentation of the fullerene [42].

The rates for dissociation reactions 5.11, 5.12 and 5.13 are low, 10^2 s^{-1}, 3.0×10^3 s^{-1} and 15×10^3 s^{-1} respectively [42]. The stability of the molecule apparently decreases during the dissociation, leading to an increase of the dissociation rate.

Another reaction between an electron and C_{60}, the electron attachment reaction [46], is more likely to take place than reaction 5.9:

$$C_{60} + e^- \rightarrow C_{60}^- \quad (5.14)$$

The energy needed for this reaction is 0.26 eV. From this fullerene ion no fragmentation has been reported. However, this ion might possible react with an argon ion, leading to dissociation of the fullerene:

$$C_{60}^- + Ar^+ \rightarrow C_2^* + C_{58} + Ar \quad (5.15)$$

We have seen that the injection of fullerene in the plasma leads to excited C_2 in the plasma. If the fragmentation degree of the fullerene does not change considerably with increasing concentration in the plasma, and the C_2 emission is linear with the amount of C_2, the C_2 emission will reflect the amount of fullerene injected into the plasma. Under the conditions that the flow of the carrier gas through the evaporator is high enough to inject all the C_{60} vapor present in the evaporator into the plasma, the amount of fullerene inside the plasma, and thus the C_2 emission, will give an indication of the vapor pressure curve of C_{60}. To check these assumptions, the emission intensities of the Swan band ($A^3\Pi \rightarrow X^3\Pi$) have been measured as a function of the temperature in the drum of the evaporator. The results are shown in figure 5.4. This figure clearly shows that the in-

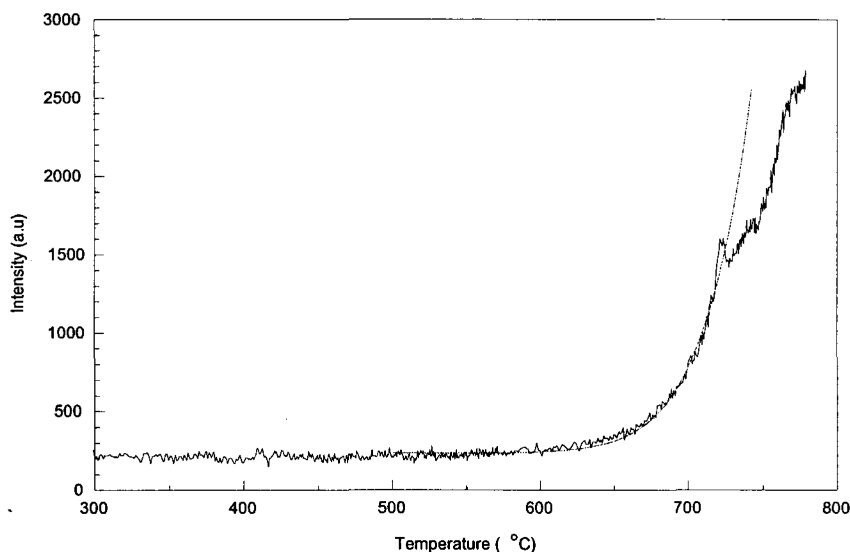

Figure 5.4: Intensity of C_2 emission at 468.48 nm ($A^3\Pi \rightarrow X^3\Pi$) as a function of the temperature in the evaporator. The argon flow through the arc is 25 scc/s and through the evaporator 10 scc/s. The arc current is 30 A, the integration time 1 s and the slit 50 μm.

tensity of the Swan bands increases with increasing temperature, thus the amount of C_{60} also increases with increasing temperature. The intensity of C_2 emission as a function of temperature ($T \leq 720^0$C) can be fitted by:

$$I = (234 \pm 3) + \frac{(1.0 \pm 0.4) \cdot 10^{16}}{T} \cdot \exp[-\frac{(18400 \pm 330)}{T}] \tag{5.16}$$

The first, temperature independent part of the equation, is the intensity of the continuous plasma and background radiation. The second, temperature dependent part gives the emission of the Swan band and, under the conditions mentioned above, should reflect the vapor pressure of C_{60} inside the evaporator. At $T = 725^0$C a deviation from the exponential behaviour is observed. This deviation may be caused by the reported change of the structure of C_{60} into amorphous carbon at temperatures higher than 700^0C [43].

The vapor pressure of C_{60} is given by [9]:

$$p = p_0 \cdot \exp[-\frac{18899}{T}] \tag{5.17}$$

The amount of C_{60} vapor in the evaporator can thus be given by:

$$[C_{60}] = \frac{p}{kT} = \frac{p_0}{kT} \cdot \exp[-\frac{18899}{T}] \tag{5.18}$$

If we compare the second part of Eq.5.16 with Eq.5.18, we see that both have the same structure, and that the exponential factors are in good agreement with each other. The intensity of the Swan band is proportional with the vapor pressure of C_{60}. We may thus conclude that the fragmentation degree of fullerene does not decrease considerably with increasing amount of fullerene inside the plasma, and that the flow of the argon carrier gas is high enough to inject all the fullerene vapor into the plasma.

To determine the evaporation rate, a time scan of the bandhead of the C_2 emission at 468.48 nm has been made during the evaporation of 0.465 gram C_{60}. The results are shown in figure 5.5. The injection of C_{60} started at $t = 30$ s. In this figure it is clearly

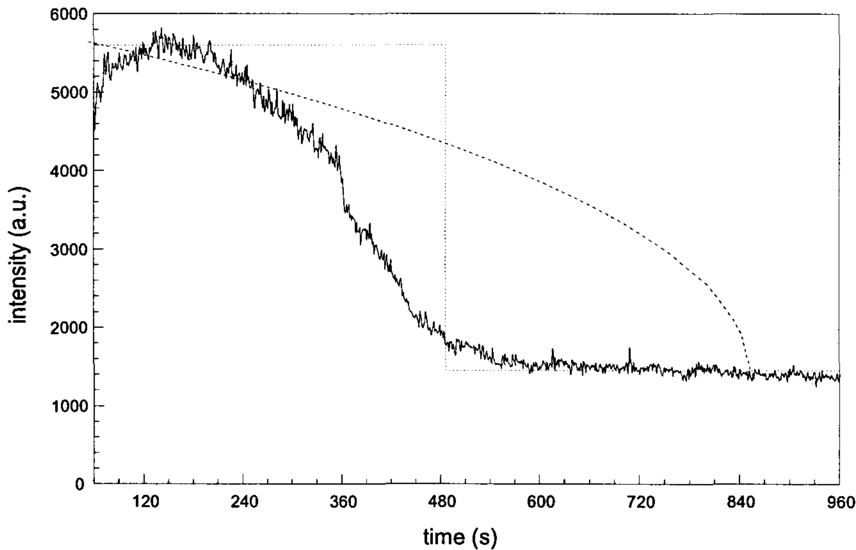

Figure 5.5: Intensity of C_2, the fragmentation product of C_{60}, as a function of time. The temperature in the evaporator is 750^0C, the argon flow through the arc 25 scc/s and through the evaporator 10 scc/s. The arc current is 30 A, the integration time 1 s and the slit 50 μm.

observed that the intensity of the C_2 emission decreases with time, indicating that the amount of C_{60} injected in the plasma is also decreasing with time. If the amount of C_{60} injected into the plasma would stay the same as long as fullerene is present in the evaporator, a discontinuity would be observed in the intensity of the C_2 emission as a function

of time (see dotted line in figure 5.5). The decrease of the evaporation rate of fullerene is caused by the decrease of the evaporation surface of C_{60} in the drum of the evaporator. This decrease of the surface is a result of the fullerene lying on the cylinder wall. As a result of the decrease of the evaporation surface, the vapor pressure, and thus the amount of C_{60} injected in the plasma, decreases (see §5.2). The dashed line in figure 5.5 gives the emission as calculated from the evaporation rate of C_{60}.

At $t \approx 480$ s the intensity reaches a constant value. This intensity is caused by the background and continuous plasma radiation. At $t = 480$ s the total amount of fullerene in the drum has been evaporated and injected in the plasma. The total time needed to evaporate 0.465 gram C_{60} is thus approximately 450 s. If we calculate the total time necessary for the evaporation, as described in §5.2, we obtain $t = 823$ s. The effective evaporation surface of the fullerene in the drum is thus 1.8 times higher than calculated. In other experiments this value may differ, because the way in which the fullerene is placed in the drum of the evaporator may differ, but this value may be used as an estimation.

In figure 5.5 it is shown that at a constant temperature, the amount of carbon injected in the plasma is not constant. When the amount of fullerene in the drum is larger than 0.5 gram, the amount of C_2 is almost constant for about 3.5 minutes (see figure 5.5). To create a depositing carbon plasma without hydrogen, with a constant carbon content, the evaporator with fullerene can be used for more than 3 minutes when the amount of fullerene in the drum is larger than 0.5 gram. These plasmas have indeed been used for deposition, as can be seen in figure 6.15, where a FTIR spectrum of a film deposited with this method is shown.

5.4 Graphite

The evaporator has also been used to vaporize graphite powder and inject it in argon plasmas. Of such a plasma an optical emission wavelength scan has been made to investigate the particles present in the plasma. A wavelength scan of an argon plasma with graphite vapor is shown in figure 5.6. In this figure the C_2 Swan bands are clearly observed, just as in the case of fullerene vapor. However, in the case of graphite, also atomic carbon lines are observed. From figure 5.6 it is clear that carbon species are injected in the plasma. Inside the plasma these carbon species form excited carbon atoms and carbon dimer molecules. The vapor pressure of graphite at 1030^0C is, however, much too small ($< 10^{-5}$Pa) to explain this amount of carbon. An explanation might be that at this temperature of 1030^0C weak bondings between clusters[1] of carbon are broken, and that these clusters form a vapor, which is injected in the plasma. Inside the plasma, these clusters are fragmented in atomic carbon and C_2, in a similar way as fullerene (§5.3).

In figure 5.7 the intensity of of the bandhead of C_2 at 468.48 nm as a function of the temperature in the drum of the evaporator is shown. In this figure it is shown that the intensity of this band first increases with increasing temperature, then decreases, and then increases again. The intensity first starts to increase at 600^0C. Apparently the weakest

[1] a string of carbon: C_N with $N > 3$

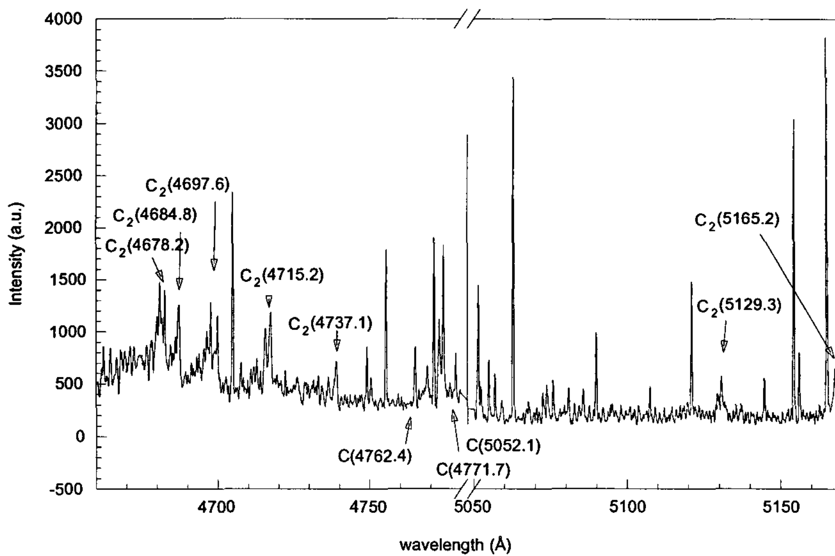

Figure 5.6: Emission spectrum of an argon plasma in which graphite vapor is injected. The argon flow through the arc is 25 scc/s and through the evaporator 10 scc/s. The arc current is 35 A, the temperature in the evaporator 1030^{0}C, the integration time 0.5 s and the slit 50 μm.

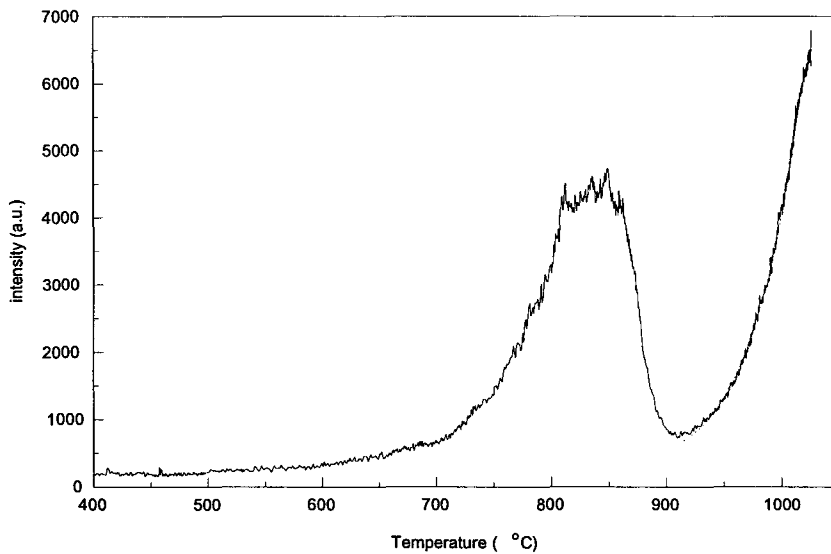

Figure 5.7: Intensity of C_2, a fragmentation product of graphite, as a function of the temperature in the evaporator. The argon flow through the arc is 25 scc/s and through the evaporator 7.5 scc/s. The arc current is 35 A, the integration time 0.5 s and the slit 50 μm.

bondings between carbon clusters are broken at this temperature and carbon clusters are vaporized. The intensity increases with the temperature, because the vapor pressure of the carbon clusters increases with temperature. At 800^0C the intensity of C_2 emission reaches a constant value and at 850^0C it starts to decrease. The cause of this might be that all carbon clusters of which the bondings were broken at 600^0C, are evaporated and injected in the plasma in the time it took to increase the temperature in the evaporator. At 900^0C the intensity starts to increase again. Apparently, again a weak bonding, slightly stronger than the former, between carbon clusters is broken and these carbon clusters are vaporized.

In this section it is shown that graphite powder may be used in the evaporator to create a depositing carbon plasma without hydrogen. Atomic carbon and C_2 are clearly observed in spite of the very low vapor pressure of graphite at this temperature. This might be explained by the breaking of weak bonds of carbon clusters in the graphite powder, and the evaporation of these carbon clusters.

Chapter 6

Graphite containing nozzle

The second way to inject carbon without hydrogen in the plasma, is with a graphite containing nozzle. With this nozzle, various plasmas have been created. In §6.1, the setup of the graphite containing nozzle and the different plasma settings are described.

To study the influence of the nozzle on the plasmas, the created plasmas have been examined by optical emission spectroscopy. In §6.2 the emission spectra will be discussed and compared with those of plasmas created with the copper nozzle, which is used normally. The plasmas created with the graphite containing nozzle are pure argon plasmas, argon-hydrogen plasmas and argon-nitrogen plasmas. In §6.3, the rotational and vibrational temperatures of argon-nitrogen plasmas created with the graphite containing nozzle, will be compared with the the rotational and vibrational temperatures of argon-nitrogen plasmas created with the copper nozzle.

Various argon-nitrogen plasmas have also been created with the graphite containing nozzle for the deposition of CN_x layers. These layers have been deposited on silicon substrates. During the deposition the layers have been examined with ellipsometry (§3.4). From simulation of the experimental data with the program 'ELLSIM' [19], the refractive index, the extinction coefficient and the growth rate of the different layers have been determined. After deposition the layers have been studied with Fourier transform infrared spectroscopy (§3.3) to investigate the different bondings present in the layer. The results of the characterization of the layers will be discussed in §6.4.

6.1 Setup of the graphite containing nozzle

Another way to get hydrogen free carbon in the plasma is with a graphite containing nozzle. The copper nozzle is replaced by a nozzle with a graphite ring (see figure 6.1). If the nozzle runs out of graphite, the ring can be replaced by another graphite ring.

In this case the graphite is introduced before the expansion. If nitrogen or hydrogen is admixed in the plasma, it may react with the graphite in the nozzle, causing *chemical etching* of the graphite from the ring, after which the reaction products will be transported towards the substrate. In this case, the amount of carbon in the plasma and the deposited

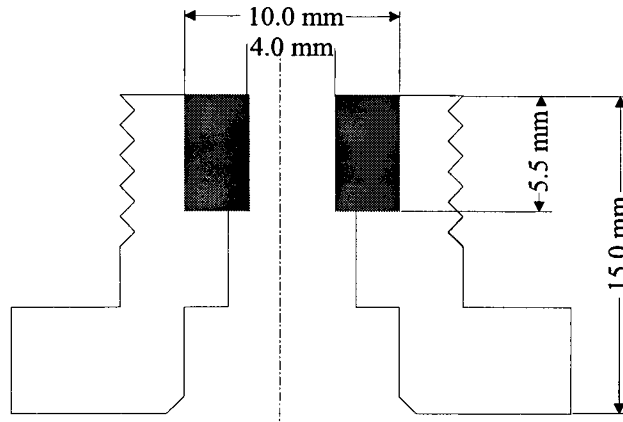

Figure 6.1: Nozzle with graphite ring

layer will depend on the nitrogen or hydrogen concentration in the plasma. The amount of carbon may also depend on the arc power, because the ionization degree and the dissociation degree change with the arc power, causing a change in the amount of reactive species at the graphite ring.

The settings of the different plasmas created with the graphite containing nozzle are listed in table 6.1 below.

Table 6.1: Settings of the plasmas created with a graphite containing nozzle.

	argon plasma	argon-hydrogen plasma	argon-nitrogen plasma
Total flow (scc/s)	100	100	100
H_2 flow (scc/s)	0	2; 5; 10	0
N_2 flow (scc/s)	0	0	5; 10; 15; 20
I_{arc} (A)	75; 87	75	48; 75; 87

6.2 Emission spectroscopy

Of the different plasmas created with a graphite containing nozzle, optical emission wavelength scans have been made, to investigate the particles present in the plasma. A wavelength scan of an argon plasma created with the graphite containing nozzle is shown in figure 6.2. The only emission lines detected in this spectrum, are argon lines. No carbon lines are observed.

In figure 6.3, a part of the emission spectrum of an argon-nitrogen plasma expanding through a graphite containing nozzle is shown. In this spectrum CN-bands ($B^2\Sigma \rightarrow A^2\Pi$, see figure 3.4) are clearly observed. Again, no carbon lines are observed. The presence

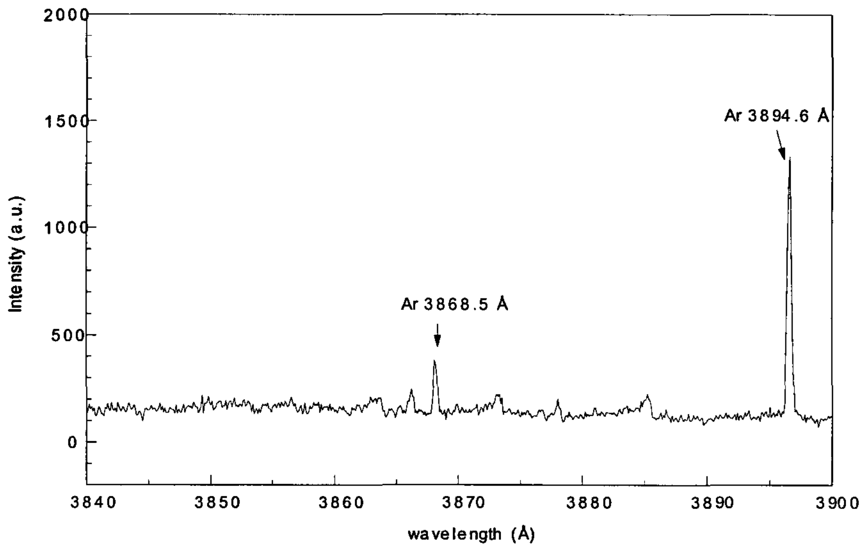

Figure 6.2: Emission spectrum of an argon plasma created with a graphite containing nozzle. The argon flow through the arc is 100 scc/s, the arc current is 75 A, the integration time is 0.3 s and the entrance slit 50 μm.

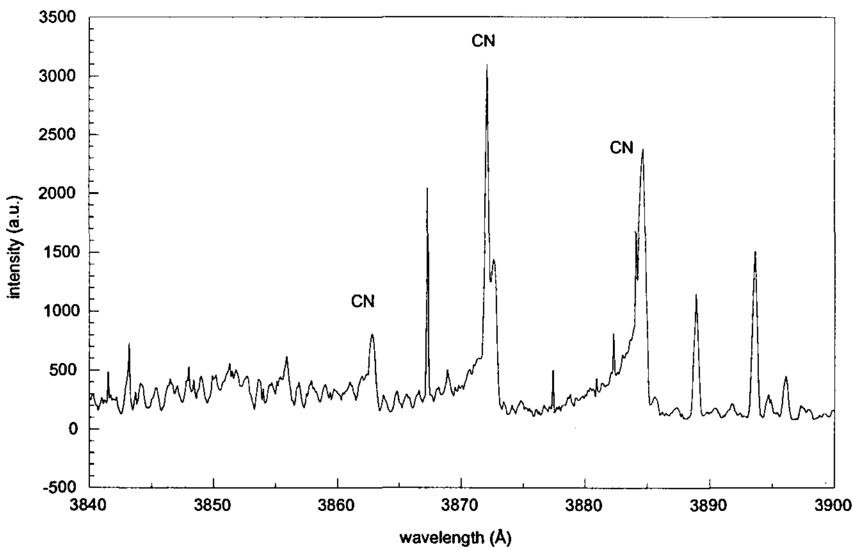

Figure 6.3: Emission spectrum of an argon-nitrogen plasma created with a graphite containing nozzle. The total flow through the arc is 100 scc/s and contains 20% nitrogen. The arc current and the entrance slit are the same as for the argon plasma (75 A and 50 μm, respectively). The integration time is 0.5 s.

of the CN-bands is most probably caused by the chemical etching of the graphite in the nozzle by nitrogen atoms. This etching of graphite may take place by the following, weakly exothermic (0.01 eV) reaction [20]:

$$C(solid) + N \rightarrow CN(gas) \tag{6.1}$$

Argon metastable atoms are known to excite molecular gasses like N_2 by energy transfer [21]. Such mechanism could explain the excitation of the CN molecules to the $B^2\Sigma$ level:

$$Ar^* + CN \rightarrow Ar + CN^*. \tag{6.2}$$

The energy needed for the excitation of CN from the ground level to the $B^2\Sigma$ level is 3.2 eV. The energy of the argon metastable atom is 11.5 eV and this energy could also cause dissociation of CN (7.8 eV needed).

A part of the emission spectrum of an argon-hydrogen plasma is shown in figure 6.4. Some very weak CH^+-bands ($^1\Pi \rightarrow ^1\Sigma$) can be observed in this spectrum, but no CH-

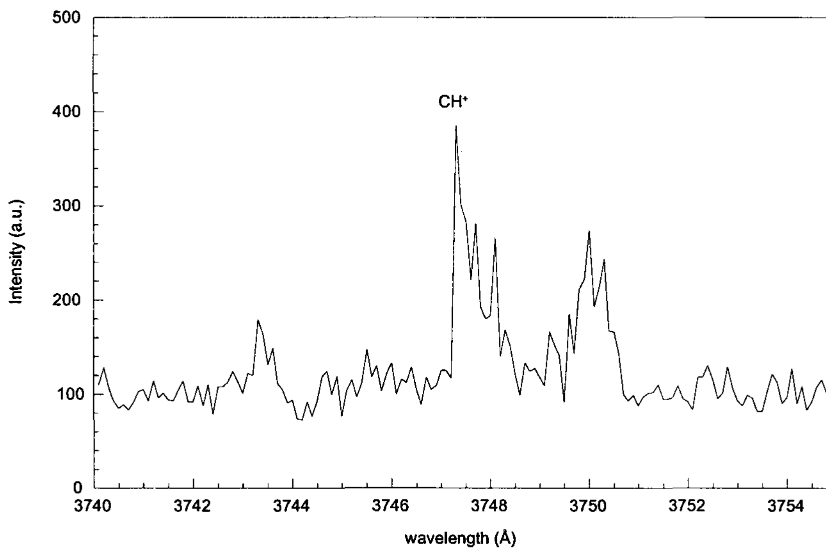

Figure 6.4: Emission spectrum of an argon-hydrogen plasma created with a graphite containing nozzle. The argon flow is 95 scc/s and the hydrogen flow is 5 scc/s. The arc current is again 75 A and the integration time is 0.5 s. The entrance slit is the same as before (50 μm).

bands are observed. Again, as in the two previous cases, no carbon lines are observed. The presence of the CH^+ band is again caused by chemical etching of the graphite, this time by the hydrogen atoms. The etching reaction may be given by the exothermal reaction [22]:

$$C(solid) + H \rightarrow CH(gas) \tag{6.3}$$

Inside the plasma charge exchange between Ar^+ or H^+ and CH (ionization energy of 10.6 eV) may occur [23]:

$$Ar^+ + CH \leftrightarrow Ar + CH^+ \quad (6.4)$$

$$H^+ + CH \leftrightarrow H + CH^+ \quad (6.5)$$

During reaction 6.4, the CH^+ ion may get excited to the $^1\Pi$ level (3.3 eV needed) by the excess of the energy of the argon ion. The excess of energy of H^+ is to low for excitation of CH^+ in reaction 6.5. However, the molecular ion formed in this reaction, may be excited to the $^1\Pi$ level by excitation exchange with argon or hydrogen [23]:

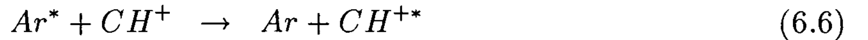

$$Ar^* + CH^+ \rightarrow Ar + CH^{+*} \quad (6.6)$$

$$H^* + CH^+ \rightarrow H + CH^{+*} \quad (6.7)$$

However, CH^+ may also recombine with an electron and dissociate:

$$CH^+ + e^- \rightarrow C + H \quad (6.8)$$

This, and the fact that the reactions 6.6 and 6.7 are in competition with the backward reactions of 6.4 and 6.5, may explain the weak intensities observed.

In all three cases no excited carbon species are observed in the plasma. It might be that carbon species are present in the plasma, but not in an excited state. However, for the excitation of the carbon atom 5.0 eV is needed and for the C_2 molecule only 2.4 eV, so these particles should easily get excited inside the plasma. This indicates that most likely no atomic or molecular carbon is present in the plasma, or at least not in a sufficient amount to be observed by emission spectroscopy, and thus hardly any dissociation of CN or CH takes place.

In the case of argon-nitrogen plasmas created with a graphite containing nozzle, deposition at an observable rate took place. In the other two cases (pure argon and argon-hydrogen plasmas) no deposition was observed.

The plasma will etch away carbon from the graphite containing nozzle, leading to an increase of the inner radius of the nozzle with time. This may cause a change in the amount of CN or CH coming out of the nozzle with time. To determine the influence of the age of the nozzle on the plasmas created, an argon-nitrogen plasma has been used with the nozzle, and the intensity of the CN-bandhead at 387.14 nm has been measured in time. In figure 6.5 the results are shown. At $t = 0$ a pure argon plasma with a flow of 90 scc/s and an arc current of 75 A has been started. After 90 seconds a nitrogen flow of 10 scc/s is added. In the first 3 minutes after the nitrogen is added, the intensity of the CN-bandhead decreases fast from 18400 to 9250 counts. After these three minutes the intensity decreases slowly to 5700 counts at t =25 minutes. The first part of the intensity I can be described by:

$$I = (7049 \pm 20) + (10505 \pm 100) \exp\left(\frac{-(t-91)}{(196 \pm 22)}\right), \ 91 \ s < t < 900 \ s \quad (6.9)$$

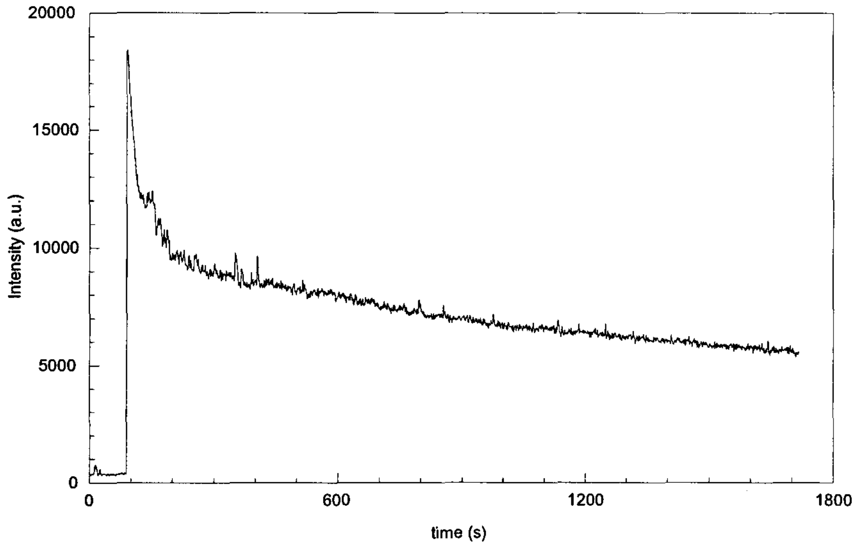

Figure 6.5: The intensity of the CN-bandhead at 387.14 nm as a function of time. The entrance slit is 250 μm, the integration time 1 s, the arc current 75 A, the argon flow 90 scc/s and the nitrogen flow 10 scc/s.

The last part of the intensity can be described by:

$$I = (8330 \pm 20) - (1.62 \pm 0.02) \cdot t, \ t > 900 \ s \tag{6.10}$$

The amount of CN inside the plasma thus decreases with the age of the nozzle. This is caused by the change of the inner diameter of the nozzle. In the beginning the plasma flows through the plasma channel with a diameter of 4 mm and enters the nozzle with a diameter of 4 mm. The plasma will chemically etch carbon from the nozzle, resulting in a larger diameter of the nozzle. The plasma will now experience less resistance from the nozzle, and as a result less carbon will be chemically etched from the nozzle, and thus less CN, or CH, will enter the plasma.

The decrease of CN in the plasma may result in a lower growth rate of the film. The total amount of nitrogen flowing through the arc however, remains the same. Because less nitrogen will be bounded with carbon to CN, more atomic and molecular nitrogen will enter the plasma. This increase of nitrogen in the plasma may result in an increase of build-in of nitrogen in the film. The atomic nitrogen inside the plasma may also cause etching of the film during deposition (see Eq.6.1). The increase of atomic nitrogen will thus also result in an increase of the etching rate and a decreasing carbon concentration in the film. These effects (the increase of build-in of nitrogen and the decrease of carbon by etching) may cause a change in the composition of the layer: the N/C ratio may increase with increasing age of the nozzle.

6.3 Rotational and vibrational temperatures

Optical emission spectroscopy has also been used to determine the rotational and vibrational temperatures of the argon-nitrogen plasmas created with a graphite containing nozzle. Just as was the case for argon-nitrogen plasmas created with a copper nozzle, the electron energy, rotational energy, vibrational energy and translational energy of the molecules inside the plasma, may not be equal. To examine the energy exchange between electrons and the rotational and vibrational energies of nitrogen, the vibrational and rotational temperatures of the plasmas have been investigated. For this, the emission spectra of the plasmas have been recorded in the DEPO I laboratory and from these data E. Aldea[1] and G. Dinescu[1] have determined the vibrational and rotational temperatures of the plasmas. The CN emission spectrum is coinciding with the N_2^+ emission at these wavelengths, so the temperatures have been determined from the $B^2\Sigma \rightarrow A^2\Pi$ transition of CN and the $B^2\Sigma \rightarrow X^2\Sigma$ transition of N_2^+. The results are shown in figures 6.6 and 6.7, respectively. The rotational and vibrational temperatures for CN and N_2^+ are assumed to be equal.

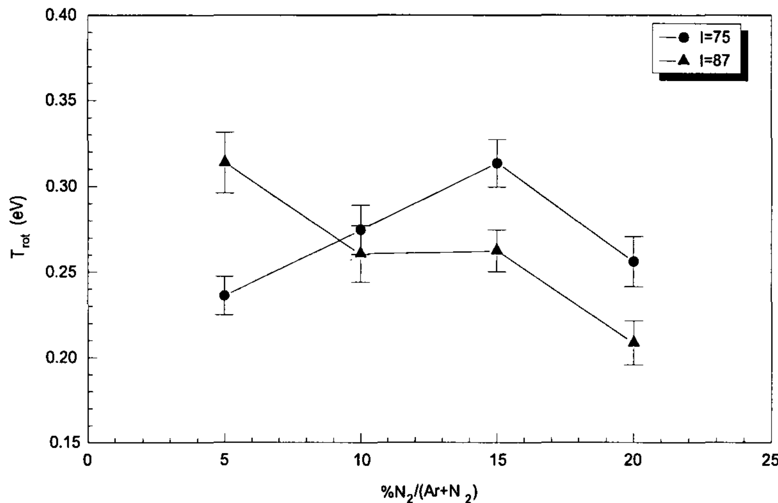

Figure 6.6: The rotational temperature of CN and N_2^+, measured 32 cm from the nozzle, as function of the nitrogen concentration. The arc currents are 75 and 87 A, the entrance slit of the monochromator was 50 μm and the integration time was 0.5 s.

In figure 6.6 it can be seen that the rotational temperature of the different plasmas varies between 0.20 eV and 0.34 eV and has no clear relationship with the composition of the plasma. The average temperature is 0.27 eV. For pure argon-nitrogen plasmas also no relationship with the composition of the plasma was observed (see figure 4.13). The average temperature of the plasma however, was 0.02 eV lower, but this difference is smaller than the uncertainty in the temperature in figures 4.13 and 6.6.

[1]Institute of Physics and Technology of Radiation Devices, Low Temperature Plasma Departement, Bucharest, Rumania

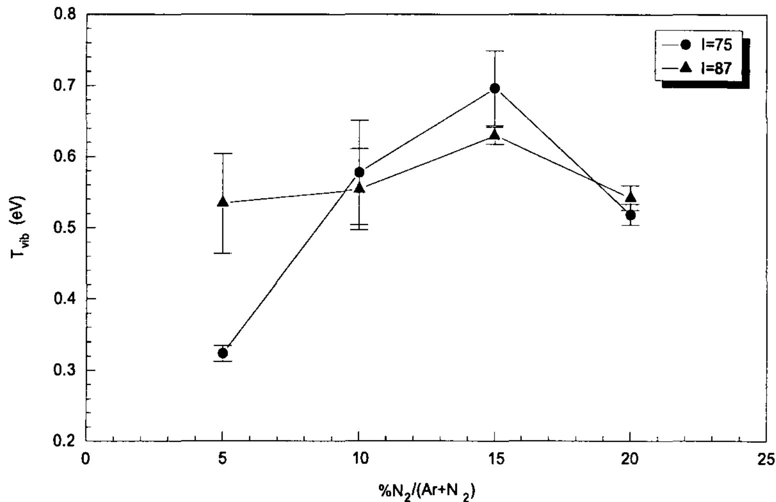

Figure 6.7: The vibrational temperature of CN and N_2^+, measured 32 cm from the nozzle, as function of the nitrogen concentration. The arc currents are 75 and 87 A, the entrance slit of the monochromator was 50 μm and the integration time was 0.5 s.

The vibrational temperature (figure 6.7) first increases with the nitrogen concentration, reaches a maximum and then decreases again. The maximum of the vibrational temperature is 0.70 eV for an arc current of 75 A and 0.63 eV for an arc current of 87 A and occurs at a nitrogen concentration of approximately 15%. If we compare the vibrational temperature with the vibrational temperature and with the electron temperature (figures 4.14 and 4.8) of argon-nitrogen plasmas created with a copper nozzle, we see a shift of the maximum from 10% in the latter two cases to 15% in the first case. The vibrational levels of a molecule can be excited by electrons. A higher electron temperature will lead to a better excitation to higher vibrational levels of the molecule and thus to a higher vibrational temperature. If we assume that the heating of the electrons is caused by the mechanisms described in §4.3 (i.e. heating of the electrons by super elastic collisions with metastable nitrogen species or the loss of mostly low energy electrons in the recombination reaction 4.4), this shift can be explained by the loss of nitrogen species in the formation of CN. If we assume that a part of the nitrogen atoms is lost in the nozzle by the formation of CN, the concentration of molecular and atomic nitrogen in the plasma decreases. The maximum of the electron temperature, caused by nitrogen species, will thus occur at a higher nitrogen flow. The mean lifetime of excited CN formed in the nozzle is too short (5 ns [12]) for super elastic collisions with electrons to occur and thus can not take over the possible heating by metastable nitrogen.

If we compare the values of the vibrational temperature of CN at a nitrogen concentration of 15% with the electron and vibrational temperature in an argon-nitrogen plasma at a nitrogen concentration of 10%, we can see that they are in good agreement with each other. Apparently the exchange between the electron energy and the vibrational energy is pretty good. The exchange between these energies and the rotational energy however, does hardly take place.

6.4 Film characterization

Plasmas created with a graphite containing nozzle have been used for deposition of carbon nitride films. For this purpose, argon-nitrogen plasmas of different composition have been used. The formation of these films is studied during deposition by ellipsometry (see §3.4). The two ellipsometric angles Ψ and Δ change during the deposition and form a curve in the $\Psi - \Delta$ plane. This curve is compared with curves simulated with the program 'ELLSIM' [19]. From the simulation the refractive index, the extinction coefficient and the thickness of the film is obtained. From the thickness of the film and the total deposition time, the average growth rate is calculated. In figure 6.8 an example of a measured $\Psi - \Delta$ curve and a simulation are shown.

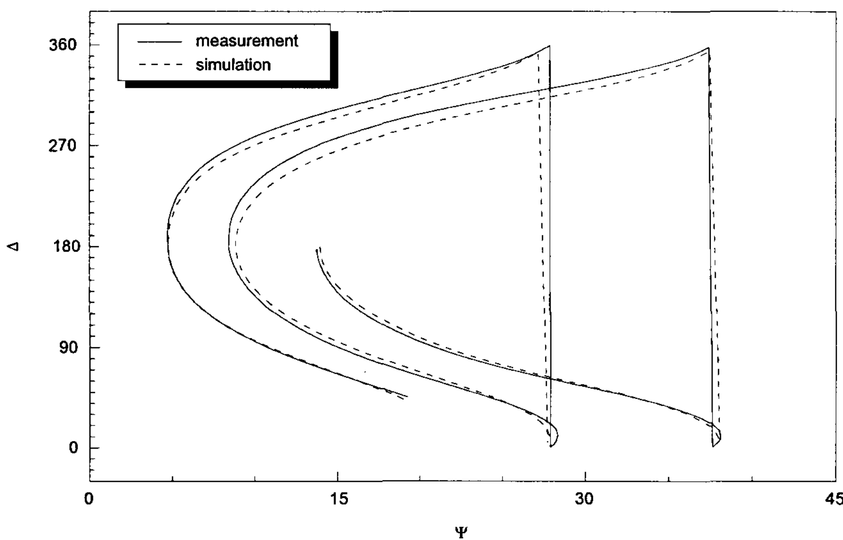

Figure 6.8: A $\Psi - \Delta$ curve measured during the deposition of a carbon nitride film and a simulation of this curve. The arc current during the deposition was 48 A, the argon flow was 80 scc/s and the nitrogen flow was 20 scc/s. The refractive index, the extinction coefficient and the thickness derived from the simulation are 1.96, -0.080 and 444 nm, respectively.

With ellipsometry the refractive index of films deposited with plasmas containing different concentrations of nitrogen (5%, 10%, 15% and 20%), have been determined. To minimize the effect of the age of the nozzle (see figure 6.5: the amount of CN decreases with increasing age of the nozzle) on the films, before each experiment a new graphite containing nozzle has been mounted in the arc. The results for the three different arc currents used (48 A, 75 A and 87 A), are given in figure 6.9 by the open symbols, connected with lines. From this figure it is clear that the refractive index of the carbon nitride film only slightly increases with increasing concentration of nitrogen in the plasma when a new nozzle is used. The value of the refractive index varies between 1.89 and 1.97. Films have also been

deposited with graphite containing nozzles which had been used in earlier experiments. The refractive index of these films is also shown in figure 6.9, denoted by the solid symbols. The refractive index of these film is much lower (between 1.72 and 1.85) than in the case of a new nozzle, as can be seen in this figure.

Earlier in this section, it has been argued that the amount of CN inside the plasma decreases with the age of the nozzle (figure 6.5) when the nitrogen flow is constant, and that this might result in an increase of the N/C ratio of the film. Deposition of films with a new nozzle might thus result in a lower N/C ratio in the films than when an old nozzle is used. According to figure 6.9, this increase of the N/C ratio due to the use of an old nozzle thus results in a decrease of the refractive index. This is in agreement with other publications, which report a decrease of the refractive index as the nitrogen content in the film increases [24] [25]. Wang and Martin [25] report that the refractive index decreases from 2.5 for pure carbon films to 2.0 for films containing 30 at.% nitrogen.

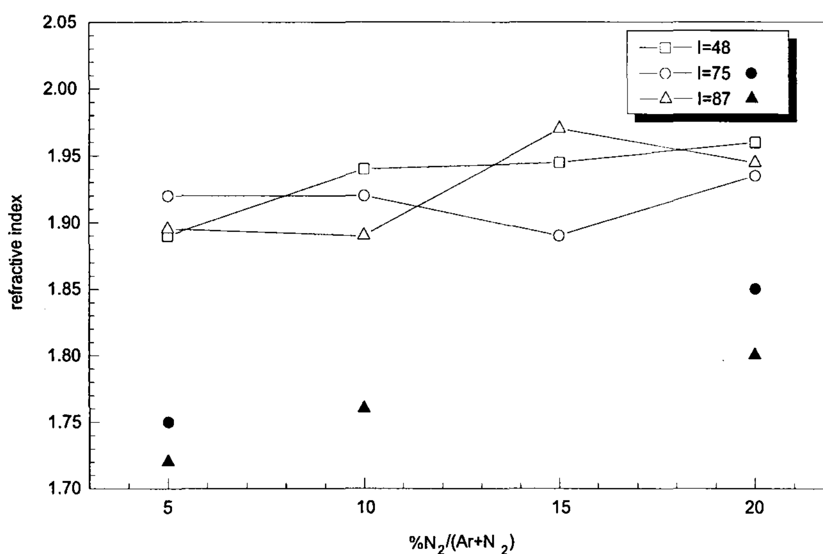

Figure 6.9: Refractive index of the carbon nitride films, obtained with ellipsometry measurements, as a function of the nitrogen concentration in the arc. The open symbols represent the depositions made with a new nozzle, the solid symbols the depositions made with an old nozzle.

Of the carbon nitrogen films deposited with the plasmas containing different nitrogen concentrations (5%, 10%, 15% and 20%), also the extinction coefficients have been determined. The results are shown in figure 6.10. The measurements of the films deposited with a new nozzle are represented by the open symbols, connected with lines. The extinction coefficient varies between -0.038 and -0.083 for the different films, but it does not show any dependency on the amount of nitrogen or the arc current used for the deposition. The extinction coefficient of the films deposited with old nozzles have also been examined. These results are represented in figure 6.10 by the solid symbols. The values for these

films lie between -0.030 and -0.049 and seem to be higher than the extinction coefficient of the films deposited with a new nozzle. The extinction coefficients might thus increase with an increasing N/C ratio of the film. This is in disagreement with Wang, Martin and Kinder [24] who report that the extinction coefficient does not change significantly with the nitrogen content in the film.

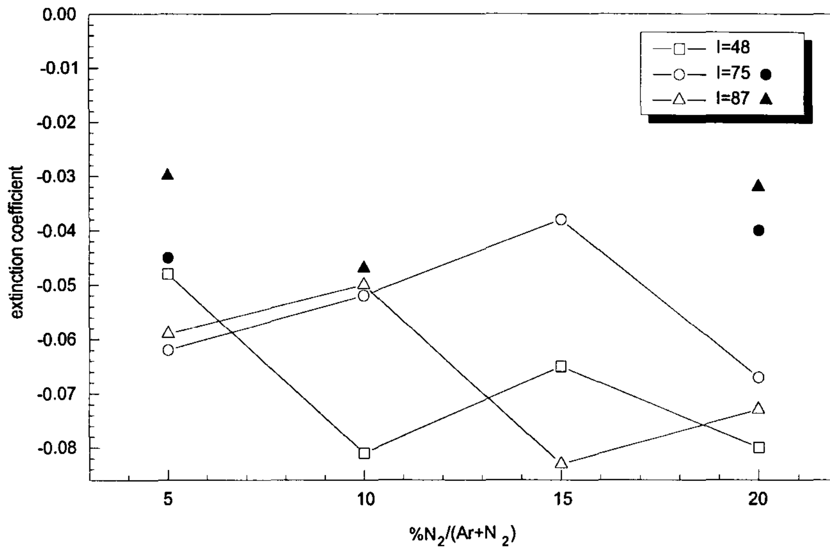

Figure 6.10: Extinction coefficient of the carbon nitride films, as determined by ellipsometry measurements, as a function of the nitrogen concentration in the arc. The arc currents used are 48 A, 75 A and 87 A.

With ellipsometry also the thickness of the films has been determined. By dividing this thickness by the deposition time, the average growth rate during the deposition is obtained. The results are shown in figure 6.11. The measurements of the films deposited with a new nozzle are represented by the open symbols. The average growth rate lies between 0.11 and 0.52 nm/s for films deposited with a new nozzle. This growth rate is much lower than the rate for deposition of a-C:H layers with the cascaded arc [26], but is in the same order as the growth rate reported for other techniques [27]. The deposition rate seems to increase with increasing nitrogen concentration, if we do not take the values at 10% nitrogen into account. The deviation at 10% is possibly caused by the difference in the nozzle used. The weight of different new graphite containing nozzles may vary by as much as 0.08 gram, while during a deposition the weight of a nozzle decreases with 0.02 to 0.05 gram. This difference in weight might be caused by differences in the amount of graphite inside the nozzle or by a different kind of graphite being used. This may result in deviations in the growth rates. The results of the growth rates for the films where an old nozzle has been used, are represented by the solid symbols in figure 6.11. These growth rates are lower than the rates with a new nozzle and lie between 0.095 and 0.13 nm/s. In the case of 10% nitrogen in the arc and an arc current of 87 A, the growth rates for the old and the new

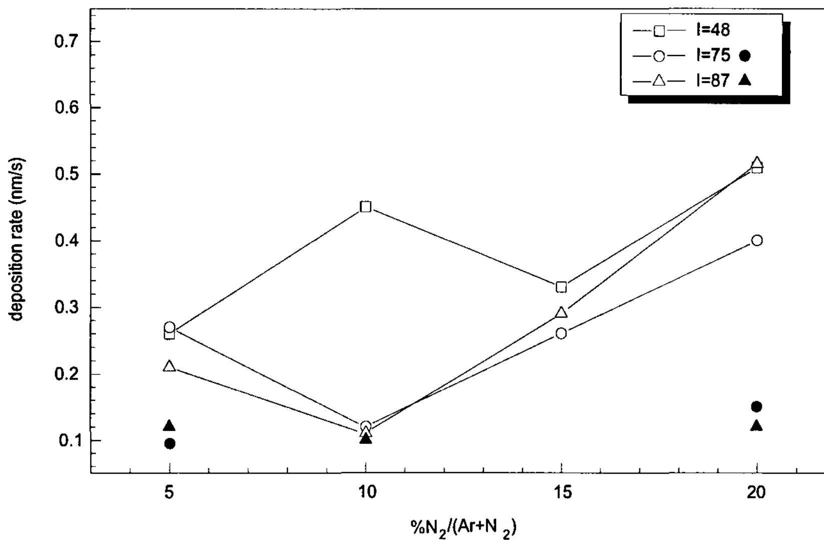

Figure 6.11: Growth rate of the carbon nitride films, as determined by ellipsometry measurements, as a function of the nitrogen concentration in the arc.

nozzle are almost the same, probably due to the deviations in the amount of graphite or the type of graphite used.

In figure 6.12, the refractive index of the deposited carbon nitride layers as a function of the average growth rate, is given. In this figure, the refractive index seems to increase with the increase of the average growth rate. The dispersion, however, is very large.

In figure 6.5 a decrease of the CN concentration with the age of the nozzle was seen. It was stated that this would lead to a decrease of the growth rate. In figure 6.13 the ellipsometric angle Ψ as a function of time is shown. It is clear that the period of Ψ increases with time and thus the increase of the thickness decreases with time (see Eq.3.20). This is caused by a decrease of growth rate in time and confirms that the growth rate decreases with the age of the nozzle. In figure 6.14, the growth rate as a function of time is given for the same experiment as depicted in figure 6.8. The growth rate for this experiment can be described by:

$$v = (0.31 \pm 0.02) + (0.84 \pm 0.03)\exp(\frac{-t}{(259 \pm 27)}) \qquad (6.11)$$

If we compare Eq.6.11 with Eq.6.9, the same exponential structure can be observed. The growth rate of the carbon nitride film is thus probably proportional to the CN emission inside the depositing plasma. The difference in the exponential factor is probably caused by the difference between the plasma settings in the two experiments.

The deposited carbon nitride films are examined by Fourier transform infrared spectroscopy (FTIR, §3.3) to analyze the bondings present in the films. A typical FTIR absorption spectrum of the deposited films is shown in figure 6.15. During deposition, the arc current was

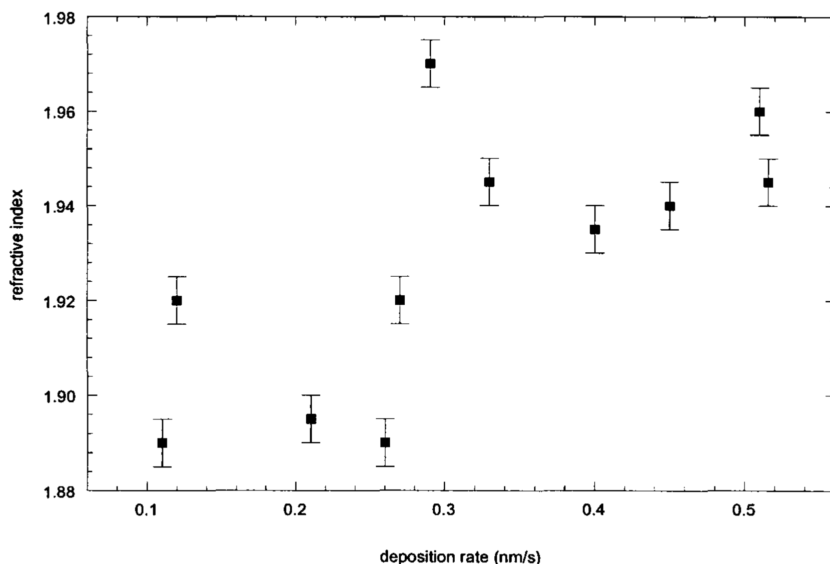

Figure 6.12: Refractive index of the carbon nitride films as a function of the growth rate.

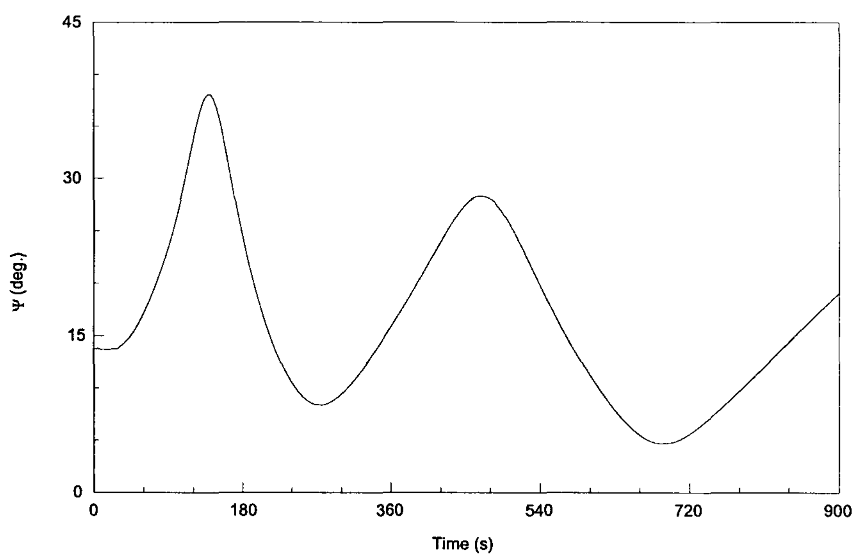

Figure 6.13: Ellipsometric angle Ψ as a function of time for the same measurement as depicted in figure 6.8.

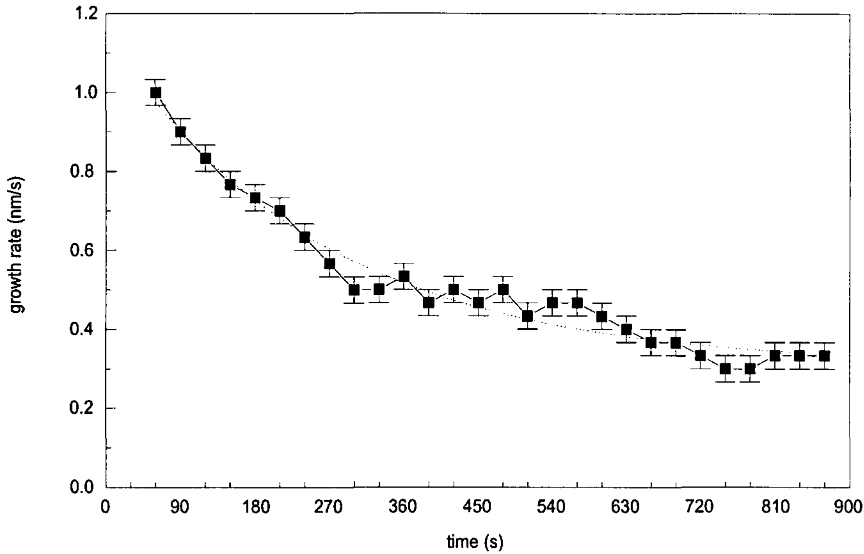

Figure 6.14: Growth rate as a function of time for the same measurement as depicted in figure 6.8.

75 A, the argon flow 90 scc/s, the nitrogen flow 10 scc/s and the substrate temperature 50^0 C. In this figure also absorption spectra of an amorphous hydrogenated carbon nitride film and an amorphous carbon film deposited with fullerene injected into an argon plasma, are shown.

Due to the low thickness of the carbon nitride film, no interference pattern can be seen in this figure, so it is not possible to determine the thickness and the refractive index of this spectrum.

In figure 6.15 several absorption peaks are visible, from which the bondings present in the films may be analyzed. The bonding of nitrogen with carbon in the a-C:N film is proven by the absorption peak at 2197 cm^{-1}, corresponding to the triple bonded CN stretching mode [28]-[33]. If we compare this with the C≡N peak of the a-C:N:H film, we can see that the amount of C≡N-bondings is lower in the a-C:N film. In the a-C:N film a broad region of absorption is visible in the region 900-1900 cm^{-1}, caused by the superposition of several bands. The top in this region lies at 1543 cm^{-1} and is not observed in the other films. This peak may correspond to double bonded CN [35]. Also NH_2 is reported to have an absorption band in this region [36][30], but no hydrogen is present in the plasma, so it is not likely to have hydrogen inside the film. On the left shoulder of the broad absorption region of a-C:N, a peak is visible at 1378 cm^{-1}. This peak may be single bonded CN [28],[35],[36],[32] or single bonded C-C [3]. This peak is also observable in the a-C film and is thus probably single bonded C-C. Further to the left of the absorption region in a-C:N, a small peak is visible around the 1195 cm^{-1}. This peak may be single bonded CN [35]-[36] or NH_2 [34], but as stated before, no hydrogen is present in the plasma thus it is not likely that this absorption is caused by NH_2. On the right side two peaks are visible at 1619 cm^{-1} and 1715 cm^{-1}. This may be double bonded CN [3],[4] or double

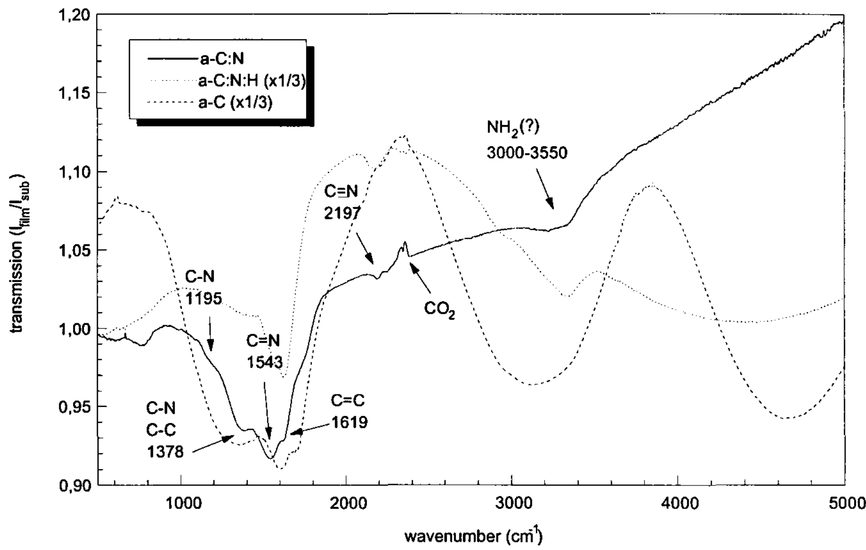

Figure 6.15: FTIR absorption spectra of an a-C:N film (solid line), an a-C:N:H film (dotted line) and an a-C film (dashed line).

bonded C=C [3],[30]. This peak is also observed in the a-C film, and is thus probably double bonded C=C. In the case of the a-C:N:H film and the a-C:N film, another broad absorption band is visible between 3000 cm^{-1} and 3550 cm^{-1}. The only bands that are reported to be in this region are the CH stretching mode at 3045 cm^{-1} [36] and the NH_2 stretching mode at 3330-3450 cm^{-1} [34],[30]. However, in the case of deposition of a-C:N, no hydrogen is present in the plasma and thus it is not likely to have NH_2 or CH absorption. The peak at 800 cm^{-1} corresponds to SiC [39] and the double peak at 2340 cm^{-1} and 2360 cm^{-1} to the CO_2 from the air.

All films deposited with a new nozzle show similar absorption peaks as in figure 6.15. Apparently the arc current and the amount of nitrogen in the arc have no noticeable influence on the bondings present in the film.

Chapter 7

Conclusions

Carbon nitride films have properties, which make them interesting for the industry. To prevent incorporation of hydrogen in the films, two methods have been developed to inject hydrogen free carbon in depositing plasmas: an evaporator for fullerene and graphite, and a graphite containing nozzle. To study the influence of the injection methods, first argon-nitrogen plasmas have been studied. Next the plasmas created with a graphite containing have been examined and are compared to plasmas created with the normally used copper nozzle. The graphite containing has also been used for deposition of carbon nitride films. Furthermore, argon plasmas in which fullerene vapor or graphite vapor is injected have been studied.

From the study of the argon-nitrogen plasmas the following conclusions can be drawn:

- The electron density decreases with increasing nitrogen concentration for arc injection, ring injection and background injection. The addition of N_2 leads to the formation of N_2^+ and this molecular ion fastly recombines with an electron, leading to the loss of an electron. By admixing more nitrogen, more N_2^+ is formed and more electrons will be lost by recombination. An increase of the nitrogen concentration will thus lead to a decrease of the electron density.

- Comparison of the experimental electron density with the electron densities calculated with a theoretical model, shows that they are in good agreement with each other for arc injection. The rate for reaction 4.3 used in the model, however, is lower than the value reported [10]. This is attributed to the model using the total N_2 concentration instead of the concentration of N_2^* in its calculation.

- In the case of ring injection and background injection, the electron densities calculated with the theoretical model, is lower than the experimental values. This may be caused by a difference in the reaction rates, due to the difference in the electron temperature, compared to arc injection.

- The neutral particle density used in the model is half the value expected. A possible explanation for the lower particle density is that the gas temperature in the vessel is

not 1000 K, as was assumed, but 2000 K. Another possible explanation is that the neutral nitrogen molecules, which are formed on the wall of the vessel, can not reach the expansion axis again, where the probe measurements are performed, because they already react on the outside of the plasma.

- The electron density decreases with the distance from the arc. This is caused by the on-going charge exchange, followed by dissociative recombination, downstream.

- The electron temperature is much higher for argon-nitrogen plasmas (0.50 - 0.63 eV) than for pure argon plasmas (0.27 - 0.40 eV). In the case of arc injection, the electron temperature has a maximum at a nitrogen concentration of 10%. A possible explanation for the increase of the electron temperature on the addition of nitrogen in the arc is that metastable nitrogen species transfer their excitation energy to the electrons by 'super elastic' collisions. Another possibility is that the electrons in the recombination reaction mainly have a low electron energy. Both the concentration of excited nitrogen species and the recombination reaction are related to the concentration of N_2^+, and the density of this molecular ion, as calculated with the theoretical model, has a maximum at 10% nitrogen admixture in the arc. When the nitrogen is injected in the ring or the background, the electron temperature increases with increasing nitrogen concentration, to saturate at 15%. Again the electron temperature can be related to the N_2^+ concentration which is calculated with the model.

- The electron temperature slightly increases with the distance from the nozzle, due to the continuous heating by metastable nitrogen or the dissociative recombination process.

- The amount of N_2^+, which is related to the amount of the excited nitrogen species, has the same dependency on the nitrogen concentration as the electron temperature. This resemblance may support the assumption that excited nitrogen species are responsible for the heating of the electrons. However, this resemblance may also indicate that higher electron temperatures cause more excitation.

- The rotational temperature of the molecular ion N_2^+ has no clear relationship with the composition of the plasma. The vibrational temperature has a similar dependency on the nitrogen concentration as the electron temperature. This indicates that the exchange between the electron energy and the vibrational energy is good, whereas the exchange between these energies and the rotational energy is hardly taking place.

From the study of plasmas in which fullerene vapor or graphite vapor is injected, the following conclusions can be drawn:

- A fragmentation product of C_{60} injected in an argon plasma, is C_2. This is in agreement with [40], [42]. Fullerene can be used to create a depositing carbon plasma without hydrogen.

- The amount of C_2 inside the plasma is related to the vapor pressure of C_{60}.

- The amount of C_{60} injected in the plasma decreases with time when only a small volume is present in the drum. This is caused by the decrease of the evaporation surface of C_{60} in the drum of the evaporator. The effective evaporation surface of 0.465 g fullerene in the drum is 1.8 times higher than the value calculated with the method described in §5.2.

- Graphite vapor will form atomic carbon and carbon dimer molecules in the plasma. Graphite powder can thus also be used to create a depositing carbon plasma without hydrogen.

- At a temperature of 1030^0C, weak bondings between clusters of carbon are broken and these clusters form a vapor, which is injected in the plasma. This explains the amount of carbon inside the plasma in spite of the vapor pressure of graphite, which is much too small to explain the observed amount of carbon.

From the study of plasmas created with a graphite containing nozzle the following conclusions can be drawn:

- The graphite in the nozzle is chemically etched by nitrogen and hydrogen. This etching results in CN and CH^+ molecules in the plasma. The graphite containing nozzle may be used for deposition of films.

- The amount of CN molecules in the plasma decreases with the age of the nozzle, which results in a decrease of the growth rate of the depositing film and possibly in a change of the N/C ratio of the film.

- The rotational temperature of CN has no clear relationship with the composition of the plasma. The vibrational temperature has a similar dependency on the nitrogen concentration as the electron temperature in argon-nitrogen plasmas created with a copper nozzle, but the maximum is shifted from 10% to 15%. This shift can be explained by the loss of a part of the nitrogen during the formation of CN, resulting in a maximum of the electron temperature, which is believed to be caused by metastable nitrogen species or the recombination of N_2^+, occurring at a higher nitrogen flow. This indicates that the exchange between the electron energy and the vibrational energy is good. The exchange between these energies and the rotational energy is hardly taking place.

From the study of the films deposited with plasmas created with a graphite containing nozzle, the following conclusions can be drawn:

- The refractive index of the carbon nitride films deposited with a graphite containing nozzle, slightly increases with increasing concentration of nitrogen. The values vary between 1.89 and 1.97.

- The increase of the N/C ratio in the plasma leads to a lower refractive index of the films (1.72 - 1.85). Films deposited with an old nozzle, which have a larger N/C ratio in the plasma, have a lower refractive index than films deposited with a new nozzle.

- The extinction coefficients of films deposited with a new nozzle varies between -0.038 and -0.083 and does not show any dependency on the amount of nitrogen used. The extinction coefficient of films deposited with an old nozzle is higher and lies between -0.030 and -0.049. The extinction coefficients thus increase with an increasing N/C ratio in the plasma.

- The growth rate of the films lies between 0.11 and 0.52 nm/s and decreases with the age of the nozzle. This growth rate is much lower than the rate for deposition of a-C:H or a-C:N:H layers with the cascaded arc. The growth rate increases with increasing nitrogen concentration and is proportional to the emission of CN bands.

- Double bonded and triple bonded CN is present in the deposited a-C:N films. The amount of C≡N is lower than in an a-C:N:H film. Absorption peaks which may be caused by both single bonded CN and double bonded CN are also observed in the FTIR absorption spectrum, however, these peaks may also be caused by single bonded C-C and double bonded C=C. These peaks are also observed in an a-C film and are thus probably caused by C-C and C=C.

Technology assessment

The industry is highly interested in films with properties like extreme hardness, wear resistance, chemical inertness, optical tunability, infra red transparency and high thermal conductivity. Some of these materials, such as diamond like carbon, amorphous carbon, boron carbide and boron nitride, are already being synthesized with a large economical impact. The study of carbon nitride, however, started only very recently. The interest in this material was initiated by publications of Liu and Cohen [1], predicting from ab initio electron structure calculations that carbon nitride may be harder than diamond. Carbon nitride is the only compound that is expected to have low deposition temperature (300^0C - 500^0C), ultra-high hardness, large band-gap (6 eV), high thermal conductivity (15 W cm^{-1} K^{-1}) and good surface roughness linked. As a consequence it has great potential for applications like tribological coatings (high density storage, hard disk manufacturing), cutting tools, thermal management of microelectronics components, and (infra red) optics.

Since the publication of Liu and Cohen many attempts have been made to synthesize carbon nitride. Most of these studies are in a non co-operative way. Under supervision of the Foundation for Fundamental Research of Matter, a framework of contacts between research teams and possible interested industries has been initiated. Within this framework operates the group Equilibrium and Transport in Plasmas at the Eindhoven University of Technology. The aim of this group is the deposition of carbon nitride films with an expanding arc plasma and the characterization of the deposition plasmas and the films.

To prevent incorporation of hydrogen, two methods to get hydrogen-free carbon in the plasma have been developed: injection of fullerene or graphite vapor in the plasma beam, and using a graphite containing nozzle in the arc instead of the copper nozzle. The influence of these methods on the plasmas and the layers deposited with these methods, have been studied during this graduation project.

Bibliography

[1] A.Y. Liu and M.L. Cohen, Phys. Rev. B 41 (1990) p. 10727.

[2] A. de Graaf, G. Dinescu, J.L. Longueville, P.D.J. van Deurzen, M.C.M. van de Sanden, D.C. Schram, J. Jonkers, E.H.A. Dekempeneer and L.J. van IJzerdoorn, *to be published.*

[3] F. Rossi, B. André and A. van Veen, J. Mater. Res. (1994) p. 2440.

[4] M. Ricci, M. Trinquecoste, F. Auguste, R. Canet, P. Delhaes, C. Guimon, G. Pfister-Guillouzo, B. Nysten and J.P. Issi, J. Mater. Res. 8 (1993) p. 480.

[5] A.J.M. Buuron, J.J. Beulens and D.C. Schram, Thin Solid Films 212 (1992) p. 282.

[6] H. Sjöström, W. Lanford, B. Hjörvarsson, K. Xing and J. Sundgren, J. Mat. Res. 11 (1996) p. 981.

[7] E. Kessels, internal report VDF/NT 96-19, Eindhoven University of Technology (1996).

[8] J. Abrefah, D.R. Olander, M. Balooch and W.J. Siekhaus, Appl. Phys. Lett. 60 (1992) p. 1313.

[9] K. Matsumoto, E. Schonherr and M. Wojnowski, J. Crystal Growth 135 (1994) p. 154.

[10] G.J.H. Brussaard, M.C.M. van de Sanden and D.C. Schram, Phys. Plasmas 4 (1997) p. 3077.

[11] D.C. Schram, *Introduction to plasmaphysics*, lecture notes, Eindhoven University of Technology.

[12] W.Lochte-Holtgreven, *Plasma diagnostics*, North-Holland Publishing Company, Amsterdam (1968).

[13] G. Ferrier, internal report VDF/NT 96-29, Eindhoven University of Technology (1996).

[14] G. Herzberg, *Spectra of diatomic molecules*, Princeton, New Jersey (1950).

[15] J.J. Beulens, *Surface modification using a cascade arc plasma source*, Ph.D. thesis (1992)

[16] E. Aldea, G. Dinescu, J.W.A.M. Gielen, M.C.M. van de Sanden and D.C. Schram, ESCAMPIG B (1996) p. 239.

[17] P. Kleuskens, internal report VDF/NT 95-15, Eindhoven University of Technology (1995).

[18] G.M.W. Kroesen, internal report VDF/NG 96-01, Eindhoven University of Technology (1996).

[19] K.G.Y. Letourneur, *Manual for ellipsometry*, Eindhoven University of Technology (1997).

[20] S. Veprek, J. Crystal Growth 17 (1972) p. 101.

[21] A. Ricard, *Reactive plasmas*, Société Française du Vide, Paris (1996).

[22] J. Küpers, Surface Science Reports 22 (1996) p.249.

[23] A. Ehbrecht, A. Kowalski and C. Ottinger, Int. J. Mass Spectrom Ion Processes 156 (1996) p. 41.

[24] X. Wang, P.J. Martin and T.J. Kinder, Thin solid films 256 (1995) p. 148.

[25] X. Wang and P.J. Martin, Appl. Phys. Lett. 68 (1996) p. 1177.

[26] J.W.A.M. Gielen, *Plasma Beam Deposition of Amorphous Hydrogenated Carbon*, Ph.D. thesis, Eindhoven (1996).

[27] M. Schaepkens, internal report, Eindhoven University of Technology (1995).

[28] H.A. Atwater, J.T. Dickinson, D.H. Lowndes and A. Polman, Mat. Res. Soc. Proc. 388 (1995) p. 271.

[29] T.Okada, S. Kamada, Y. Takeuchi and T. Wada, J. Appl. Phys. 78 (1995) p. 7416.

[30] H. Han and B.J. Feldman, Sol. State Comm. 65 (1988) p. 921.

[31] M.G. Krishna, K.R. Gunasekhar and S. Mohan, J. Mater. Res. 10 (1995) p. 1083.

[32] J.H. Kaufmann, S. Metin and D.D. Saperstein, Phys. Rev. B 39 (1989) p. 13053.

[33] H. Xin, W. Xu, X. Shi, H.Zhu, C. Lin and S. Zou, Appl. Phys. Lett. 66 (1995) p. 3290.

[34] A. Grill and V. Patel, Diamond Films Techn. 2 (1992) p. 61.

[35] Y. Taki and O. Takai, J. Appl. Phys. (1996)

[36] A. Bousetta, M. Lu, A. Bensaoulo and A. Schultz, Appl. Phys. Lett. 65 (1994) p. 696.

[37] S.V. Deshpande, J.L. Dupuie and E. Gulari, Appl. Phys. Lett. 61 (1992) p. 1420.

[38] S. Yamamoto and M. Migitaka, Jap. J. Appl. Phys. 31 (1992) p. 348.

[39] K. Kawamura, S. Ishizuka, H. Sakaue and Y. Horiike, Jap. J. Appl. Phys. 30 (1991) p. 3215.

[40] D.M. Gruen, S. Liu, A.R. Krauss and X. Pan, J. Appl. Phys 75 (1994) p. 1758.

[41] V.V. Alfrosimov, A.A. Basalaev and M.N. Panov, Tech. Phys. 41 (1996) p. 412.

[42] D.H. Yu, L.H. Andersen, C. Brink and P. Hvelplund, Z. Phys. D 29 (1994) p. 53.

[43] E. Martens and P. Peeters, internal report VDF/NT 96-09, Eindhoven University of Technology (1996).

[44] M.C.M. van de Sanden, *The expanding plasma jet: Experiments and model*, Ph.D. thesis, Eindhoven (1990).

[45] R.P. Dahiya, M.J. de Graaf, R.J. Severens, H. Swelsen, M.C.M. van de Sanden and D.C. Schram, Phys. Plasmas 1 (1994) p. 2086.

[46] D. Strele, C. Winkler, P. Krumm and R. Schrittwieser, Plasma Sources Sci. Technol. 5 (1996) p. 603.

[47] Y. Zhang, Z. Zhou, and H. Li, Appl. phys. Lett. 68 (1996) p. 634.

[48] H.K. Woo, Y. Zhang, S.T. Lee, C.S. Lee, Y.W. Lam and K.W. Wong, Diamond and Related Materials 6 (1997) p.635.

[49] J.B. Hasted, *Physics of atomic collissions*, Butterworth, London (1972).

Appendix A

The flow controller for the evaporator

To inject carbon inside the plasma, an evaporator has been constructed. To get the vapor inside the plasma, a gas flow through the evaporator has to be effectuated. To regulate this flow a Bronkhorst flow controller (type F-201C-FA) is used. The operation of the flow controller is described in §A.1. The gas used is argon and the calibration of the flow controller for argon is described in §A.2.

A.1 Operating the flow controller

The flow controller is operated with a box of which a schematic overview is given in figure A.1. The power supply (220 V) is connected at X1 and the box can be turned on/off

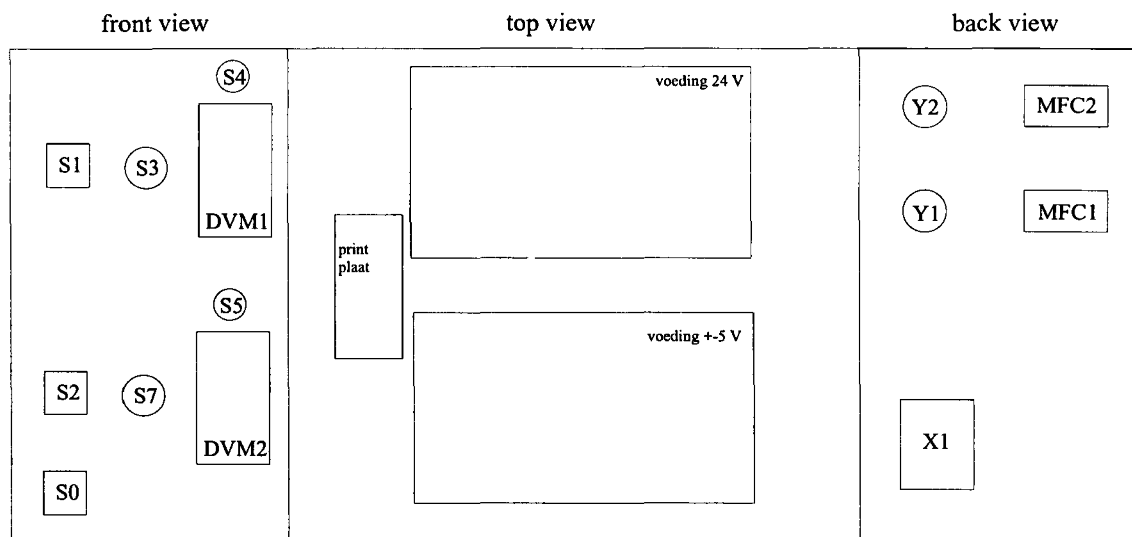

Figure A.1: The operation box of the flow controller

with switch S0. The flow controller is connected to the back of the box at MFC1. The flow through the evaporator can be adjusted with S6. If the switch S4 is set to "setpoint", DVM1 shows the setpoint of the flow controller. If it is set to "output", DVM1 shows the output value of the flow controller. From this value the actual flow can be determined (see §A.2). The switches S5 and S7 and the screen DVM2 can be used in the same way for a second flow controller which can be connected at MFC2. The switches S1 and S2 can be used to operate valves which can be connected at Y1 and Y2.

A.2 Calibration of the flow controller

The flow controller has been calibrated for argon by setting the operation box to a specific value and measuring the pressure change in the vessel as a function of time. For the vessel at DEPO 1 the relation between the flow (F, in scc/s), the pressure change (Δp, in mbar) and the time in which this pressure change takes place (Δt, in seconds) is given by the formula [26]:

$$F = 168\frac{\Delta p}{\Delta t} \tag{A.1}$$

The results of the calibration are given in table A.1 and figure A.2. Before every measurement the pressure in the vessel is 0.000 mbar. If there is no flow through the flow controller, the pressure in the vessel increases every 5 seconds with 0.001 mbar. This corresponds to a flow of $2 \cdot 10^{-4}$ scc/s and can be neglected. The argon flow through the evaporator (in

Table A.1: Calibration of the flow controller

output ± 0.01	pressure (mbar) ± 0.1	time (s) ± 0.5	flow (scc/s)
0.25	7.0	293.9	4.00 ± 0.06
0.50	25.0	531.0	7.90 ± 0.05
0.99	28.0	300.0	15.68 ± 0.06
1.50	25.0	175.5	23.94 ± 0.10
2.00	50.0	267.6	31.39 ± 0.06
2.50	50.0	211.7	39.68 ± 0.08
3.00	75.1	268.2	47.04 ± 0.06
4.00	90.0	236.5	63.92 ± 0.07
4.88	90.1	187.8	80.50 ± 0.09

scc/s) as function of the output of the operation box can be determined from a linear fit (see figure A.2) and is given by:

$$F = 16.30 \cdot output - 0.64 \tag{A.2}$$

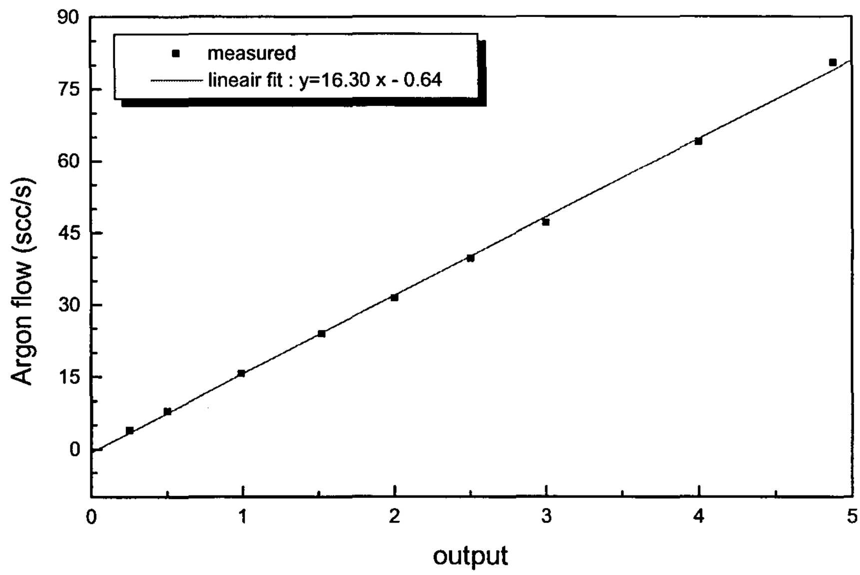

Figure A.2: Calibration of the flow controller

Appendix B

Operating box for the evaporator

To control the temperature and the cooling water of the evaporator and the valve separating the evaporator from the vacuum vessel, an operating box has been designed. A schematic overview of this operating box is given in figure B.1.

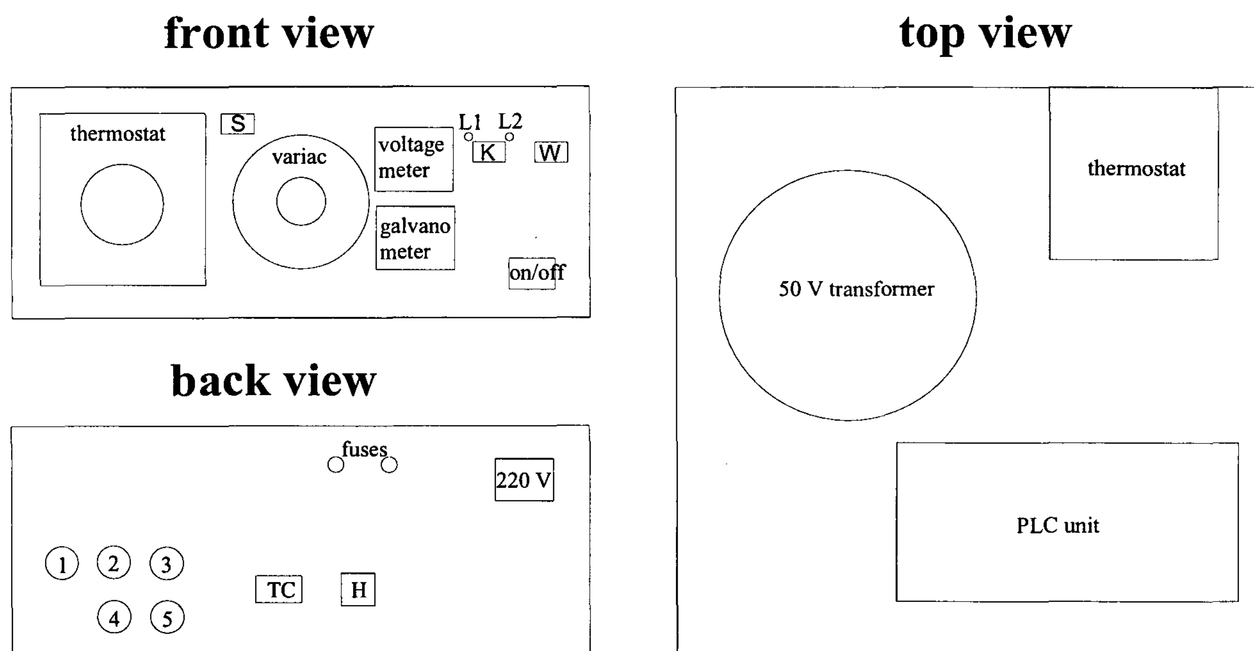

Figure B.1: Operating box

The box contains a 50 Volt transformer which supplies the power for the heating element, a thermostat for regulation of the temperature inside the evaporator, and a PLC unit controlling the valve, the water cooling and the heating element of the evaporator. When the evaporator is in the hindmost position, the valve can be opened and closed with the switch K. If the valve is open, LED L1 will light up, if the valve is closed, LED L2. When the connection between the box and the valve is missing, L1 and L2 will blink. The

water cooling can be switched on and off with switch W. If the water cooling is on, the light of the switch is on. If the light is blinking, the water cooling is not working properly. When the evaporator is not in the hindmost position and the water cooling is switched on, it can be switched on with switch S. When it is switched on, the light of the switch is on. When the evaporator is tried to switched on in the hindmost position, this light will blink. The temperature inside the evaporator is controlled with the thermostat. With the variac the power of the heating element, and thus the speed of the temperature rise, can be regulated. The voltage over and the current through the heating element can be read from the voltagemeter and the galvanometer. The connections 1 to 5 at the back of the box are for the valve, the water cooling and the position of the evaporator, connection TC is for the thermocouple, and connection H is for the heating element.

Appendix C

Listing for the Ar-N_2 model

```
program odeiv1ex(inp, out);

{$f+}

uses ode
{$IFDEF WINDOWS}
     , WinCrt
{$ENDIF}
;
const k1=1e-4; {reaction rate for N+ + N2 -> N + N2+}
      k2=7e-5; {reaction rate for Ar+ + N2 -> Ar + N2+}
      k3=1e-1; {reaction rate for N2+ + e -> N + N*}
      v=1000;  {velocity of the plasma in m/s}
      p=20;    {measuring position in cm}


      {all other parameters in micrometers and microseconds}


var
   out, out2, out3, out4                        :text;
   y0, y1                                        :array[0..1000] of real;
   i,j,n, term                                   :integer;
   a, b, d, ya, x0, x1, ae, n0, a0, perc,ar,np,n2 :real;
   {a=starting time;
    b=ending time, calculated from position and velocity of the plasma;
    d=distance per time step for calculation;
    n0= N+ density in the arc;
    a0= Ar+ density in the arc;
    perc = N2 percentage of the flow;
```

```
    np= N+ density at given position;
    ar= Ar+ density at given position;
    n2= N2+ density at given position;
    others: needed for program odeiv1;
    }
   fonam2, foname, fonam3, fonam4                 : string[12];

function f(x, y: real): real;
{function f for odeiv1:
     y'=f(x,y), x in [x0,x1]; y(x0)=number; calculate y(x1);
}
begin
  f:=n2*k1*n0*exp(-k1*n2*x)+n2*k2*A0*exp(-k2*n2*x)-k3*(n0*exp(-k1*n2*x)
                             +A0*exp(-k2*n2*x)+y)*y;
end; {f}

 begin
    foname:='p12-Ar.dat';  {file for Ar+ density as function of %N2}
    fonam2:='p12-Np.dat';  {file for N+ density as function of %N2}
    fonam3:='p12-N2.dat';  {file for N2+ density as function of %N2}
    fonam4:='ne-32a.dat';  {file for electron density as function of %N2}
    assign(out, foname); rewrite(out);
    assign(out2, fonam2); rewrite(out2);
    assign(out3, fonam3); rewrite(out3);
    assign(out4, fonam4); rewrite(out4);
    a:=0;
    b:=10000*p/v;
    n:=10; ya:=0; ae:=1e-3; d:=(b-a)/n;
    i:=0; term:=1; x0:=a; y0[0]:=ya;
    while (i<n) and (term=1) do
      begin
        writeln;
        i:=i+1; x1:=x0+d;
        for j:=0 to 100 do
        begin
          write('.');
          perc:=j/100;
          n2:=1000*perc;                {density of N2 in the vessel
                                         calculated from the total gas
                                         density inside the vessel (1000)
                                         times the nitrogen percentage.
                                         The total gas density is
                                         calculated from p=nkT}
```

```
        n0:=27*2.3*(perc/(1-perc))/(1+2.3*(perc/(1-perc)));
        a0:=27-n0;
              {27=electr.density of a pure argon plasma}
        odeiv1(f, x0, y0[j], x1, y1[j], ae, term);
              {calculation of N2+ density}
        ar:=a0*exp(-k2*n2*x1);
              {calculation of Ar+ density}
        np:=n0*exp(-k1*n2*x1);
              {calculation of N+ density}
        if i=n then
        begin
           writeln(out,perc,'  ',ar);
           writeln(out2,perc,'  ',np);
           writeln(out3,perc,'  ',y1[j],'  ');
           writeln(out4,perc,'  ',y1[j]+n0*exp(-k1*n2*x1)
                                      +A0*exp(-k2*n2*x1),'  ');
           writeln(perc,'  ',y1[j]+n0*exp(-k1*n2*x1)+A0*exp(-k2*n2*x1));
        end;
        y0[j]:=y1[j];
      end; {j}
        x0:=x1;
    end; {i}
  if term <> 1
  then
    writeln(out,' proces terminated,', ' term = ',term:1);
  close(out);
  close(out2);
  close(out3);
  close(out4);
  writeln;writeln;
  writeln('Finished');
end.
```